TAMPERE UNIVERSITY OF TECHNOLOGY

TUOMAS JULIN

FLEXO-PRINTED PIEZOELECTRIC PVDF PRESSURE SENSORS

Master of Science Thesis

Examiners:
Professor Helge Lemmetyinen
Doctor Sampo Tuukkanen
Examiners and topic approved in the
Science and Environmental
Engineering Faculty Meeting
December 7th, 2011

ABSTRACT

TAMPERE UNIVERSITY OF TECHNOLOGY
Master's Degree Programme in Science and Engineering
TUOMAS JULIN: Flexo-printed piezoelectric PVDF pressure sensors
Master of Science Thesis, 61 pages, 8 Appendix pages
April 2012
Major: Chemistry
Examiner: Helge Lemmetyinen, Sampo Tuukkanen
Keywords: flexography, printed electronics, PVDF, piezoelectric pressure sensor

The main focus in this thesis was to study the suitability of flexographic printing and new electrode materials in the manufacture of flexible piezoelectric pressure sensors. There are numerous application where flexible and economical pressure sensors can be used. Such are process controll in industry and measurement of vital functions and pressure stress in health care. Flexography would enable economical and efficient mass-production of such sensors.

Function of the pressure sensors fabricated in this work is based on piezoelectricity of the uniaxially stretched and poled polyvinylidene fluoride (PVDF) that is used as substrate in sensors. When piezoelectric PVDF is exposed to mechanical stress, electric charges of opposite signs (voltage difference) form on opposite sides of the substrate. If conducting electrodes are fabricated on surface of the substrate, formed charges can be conducted to measuring unit that analyses the magnitude of the charge. Because formed charge is proportional to the force applied on PVDF, force or pressure applied on sensor can be solved.

Because piezoelectric PVDF cannot resist high temperatures, no inks that require high sintering temperatures can be used as electrode materials. Manufacture of metal electrodes by sputtering or evaporation is slow and expensive. In this work carbon nanotubes and conducting poly(3,4-ethylenedioxythiophene) polymer are studied as alternative electrode materials. Electrodes are fabricated by using RK Flexiproof 100 flexo-printer or CX202 Motorized bar coater. For lower price and better availability also non-piezoelectric substrates were used to evaluate printing process and electrode materials.

Fabricated samples were electrically characterized. Main focus was in sheet resistance of the electrodes and sensitivity of the sensor elements. Obtained sheet resistance values varied a lot. Highest values were up to over four orders of magnitude larger than those of metal electrodes. Despite the high sheet resistance, fabricated samples showed sensitivities comparable to reference samples. According to the results of this work, studied new electrode materials are most likely suitable to be used in flexible pressure sensors.

TIIVISTELMÄ

TAMPEREEN TEKNILLINEN YLIOPISTO
Teknis-luonnontieteellinen koulutusohjelma
TUOMAS JULIN: Flexo-printed piezoelectric PVDF pressure sensors
Diplomityö, 61 sivua, 8 liitesivua
Huhtikuu 2012
Pääaine: kemia
Tarkastajat: Helge Lemmetyinen, Sampo Tuukkanen
Avainsanat: flexopaino, painettava elektroniikka, PVDF, pietsosähköinen paineanturi

Tämän opinnäytetyön tarkoituksena oli tutkia flexopainon ja uusien elektrodimateriaalien soveltuvuutta taipuisien pietsosähköisten paineantureiden valmistuksessa. Taipuisille ja edullisille paineantureille löytyy lukuisia sovelluskohteita, kuten teollisuuden prosessinvalvonta ja elintoimintojen sekä painerasituksen mittaaminen terveydenhuollossa. Flexopainaminen mahdollistaisi tällaisten antureiden edullisen ja tehokkaan valmistuksen massatuotannossa.

Työssä valmistettujen paineanturien toiminta perustuu substraattina käytetyn uniaksiaalisesti venytetyn ja polarisoidun polyvinylideenifluoridin (PVDF) pietsosähköisyyteen. Pietsosähköisen PVDF substraatin pinnalle, kalvon eri puolille, muodostuu erimerkkiset sähkövaraukset (jännite-ero) kun tähän materiaaliin kohdistetaan mekaaninen voima. Jos substraatin pinnalle valmistetaan sähköä johtavat elektrodit, saadaan muodostuneet varaukset johdettua mittalaitteistoon, joka analysoi varauksen suuruuden. Koska muodostuneen varauksen suuruus on verrannollinen PVDF:ään kohdistuneeseen voimaan, saadaan anturiin kohdistunut voima tai paine ratkaistua.

Koska pietsosähköinen PVDF ei kestä korkeita lämpötiloja, ei elektrodimateriaaleina voida käyttää korkeita sintrauslämpötiloja vaativia musteita. Metallisten elektrodien valmistaminen sputteroimalla tai höyrystämällä on puolestaan hidasta ja kallista. Tässä työssä vaihtoehtoisina elektrodimateriaaleina tutkitaan hiilinanoputkia ja johtavaa poly(3,4-etyleenidioksitiofeeni) polymeeriä. Elektrodit valmistetaan joko RK Flexiproof 100 fleksopainokoneella tai CX202 Motorised bar coater musteenlevityslaitteella. Halvemman hinnan ja helpomman saatavuuden takia näytteitä painettiin myös ei-pietsoelektrisille substraateille, joilla voitiin tutkia painoprosessia ja elektrodimateriaalien ominaisuuksia.

Valmistettujen näytteiden ominaisuuksista tutkittiin etenkin elektrodien neliöresistanssia ja herkkyyttä. Neliöresistanssien arvot vaihtelivat suuresti, ollen jopa yli nelja kertaluokkaa suurempia kuin metallisilla elektrodeilla. Korkeasta neliöresistanssista huolimatta valmistettujen näytteiden herkkyydet olivat samaa suuruusluokkaa referenssiantureiden kanssa. Tästä työstä saatujen tulosten perusteella tutkitut uudet elektrodimateriaalit soveltuvat todennäköisesti käytettäviksi taipuisissa paineantureissa.

PREFACE

The work for this thesis was done in Organic Electronics group at the Department of Electronics at Tampere University of Technology. The work was done starting from March until the end of 2011 as part of a project funded by the Academy of Finland.

I would like to thank my supervisor and examiner Ph.D. Sampo Tuukkanen for the post in his project and for all the help he gave me during this work. I also would like thank my other examiner Prof. Helge Lemmetyinen for his help on this work. I thank Prof. Donald Lupo for being a nice and helpful boss.

I thank Petri, Santtu, Miao, Marika, Kaisa, Eerik, Esa, Juha, Iiro and Lauri for their help and pleasant working environment. Especially I want to thank Suvi, my fellow chemist, for being helpful and a chemist.

I thank all the other co-workers of the Department for the helpful and happy working environment.

I thank collaborators Pasi Moilanen from (JYU) and Ville Rantanen (TUT) for their time, work and help on this work.

I thank Juvenes personnel for providing me daily with good tasty food, spiced with friendly service. I also thank Riitta Myyryläinen, secretary of Faculty of Science and Environmental Engineering for being a true student-friendly person.

I thank my family and especially my grandmother Raija, for support and encouragement throughout my studies starting from elementary school. I also thank all my friends for all the good times. Finally, I thank my girlfriend Anu for her love and support.

CONTENTS

LIST OF SYMBOLS AND ABBREVIATIONS

γ	surface tension
γ_{GL}	interfacial tension of gas-liquid interface
γ_{GS}	interfacial tension of gas-solid interface
γ_{LS}	interfacial tension of liquid-solid interface
θ	contact angle
μ	dipole moment
ρ	resistivity
A	cross sectional area of conductor
C	capacitance
$\mathbf{C}_h$	chiral vector of SWNT
D	dielectric displacement
d_t	diameter of SWNT
E	electric field
G	geometric correction factor
I	current
L	length of conductor
L_c	length of chiral vector of SWNT
F	force
R	resistance
R_C	contact resistance
R_{DUT}	resistance of device under test
R_S	sheet resistance
R_W	wire or probe resistance
s	spacing of probes
t	thickness of film
T	temperature
$\mathbf{T}$	translational vector of CNT
V	voltage
W	width of film
x	strain
X	stress

ADC	analog-to-digital converter
AFM	atomic force microscope
CMC	carboxymethyl cellulose
CNT	carbon nanotube
CP	conducting polymer
DMSO	dimethylsulfoxide
DUT	device under test
EG	ethylene glycol
IPA	isopropanol
MWNT	multi-walled carbon nanotube
OM	optical microscope
PC	polycarbonate
PCB	printed circuit board
PE	polyethylene
PEDOT	poly(3,4-ethylenedioxythiophene)
PEDOT:PSS	poly(3,4-ethylenedioxythiophene):poly(styrenesulfonate)
PET	polyethylene terephthalate
PGMEA	propylene glycol monomethyl ether acetate
PSS	poly(styrenesulfonate)
PVC	polyvinylchloride
PVDF	polyvinylidene fluoride
SDS	sodium dodecyl sulfate
SEM	scanning electron microscope
STDEV	standard deviation
SWNT	single-walled carbon nanotube
UV	ultraviolet

1. INTRODUCTION

Flexibility and printability are rather new words in the world of electronics. Rigid circuit boards with rigid components have been around for decades and they have served us in numerous important applications. Nowadays, however, they have a worthy competitor on the market: Printed electronics, which enables even roll-to-roll mass production on flexible substrates.

In printed electronics circuits and components are printed with conventional printing methods that are familiar in graphic printing such as ink-jet, gravure, screen and flexography. Properties of the inks used in printed electronics differ remarkably from those used in graphic printing, though. Although the performance of printed electronics does not usually compete with traditionally produced electronics, performance is often good enough to be used in many applications. The benefits of printed electronics are lower cost and faster manufacture. Circuits can also be printed on flexible substrates such as polymer films, which enable their use in application where flexibility is required. [1]

It is not always just the ink that has functionality in printed electronics, but also the substrate it is printed on may be functional, as is the case with piezoelectric polyvinylidene fluoride (PVDF). Flexible pressure sensors can be manufactured by printing conducting electrodes on flexible and piezoelectric PVDF substrate. These sensors can be used, for example, to measure the pressure that the sole experiences in a shoe. Results of the measurements can be used to prevent possible pressure ulcers that may occur due to too high pressure. Pressure ulcers occur commonly in people that suffer from diabetes. [2]

One goal of this work is to find conducting inks that do not need to be sintered in high temperatures. This is because piezoelectric PVDF substrate shrinks and loses its piezoelectricity when exposed to too high temperature as Kärki et al. have experienced in their study [2]. Main focus was on inks that were based on carbon nanotubes (CNT) or poly(3,4-ethylenedioxytheophene) polystyrenesulfonate (PEDOT:PSS). Another goal is to formulate these inks so that they could be printed with flexographic press. This would enable fast and inexpensive roll-to-roll mass production of these sensors in the future.

2. FLEXOGRAPHY AND BAR COATING

Flexographic printing or flexography uses flexible relief plates to transfer desired image on substrate. The beginning of flexographic printing dates back to the late 19th century, when the first aniline press was built in 1890 in Liverpool. In the beginning of 20th century the aniline press was further improved, but it was only in 1938 when anilox roll was introduced to improve the ink metering. In the early years flexography was called aniline press because of the use of aniline dye inks. The name flexography was adopted in the 1950s. Flexography is the fastest growing conventional printing process used today. [3, pp. 75–76; 4]

What makes flexography so popular are the facts that it can be used for printing on various substrates and it is fairly inexpensive to be used even for quite small batches, because the printing plates are fairly inexpensive. For the reason that flexographic press is capable of printing on many different substrates, it is widely used especially in packaging industry, to print on carton, cardboard, plastic wrappings etc. The range of inks that can be used in flexography is also wide. Fairly low resolution due to soft printing plates and harmful characteristics of some solvents in inks are disadvantages of flexography. [3, pp. 75–88; 4]

2.1 Function and parts of flexographic press

The structure and the basic operational principle of a flexographic press are quite simple. The main parts of the press are anilox roll, doctor blade, plate cylinder, flexographic plate and impression cylinder. Flexographic press is illustrated in figure 2.1. [3, p. 80; 4]

During the printing process, first, ink is supplied to the anilox through an ink fountain or by an ink fountain roll. Second, excess ink is removed from anilox by doctor blade. Next, ink is transferred from anilox roll to flexo plate that is attached to the plate roll. Finally, the ink is transferred to a substrate fixed on impression cylinder. Structure and function of different parts of flexographic press are further described below. [3, p. 76; 4]

2.1.1 Anilox

The function of anilox is to measure and transfer adequate amount of ink to flexographic printing plate. Steel, copper, brass and ceramics are the most common

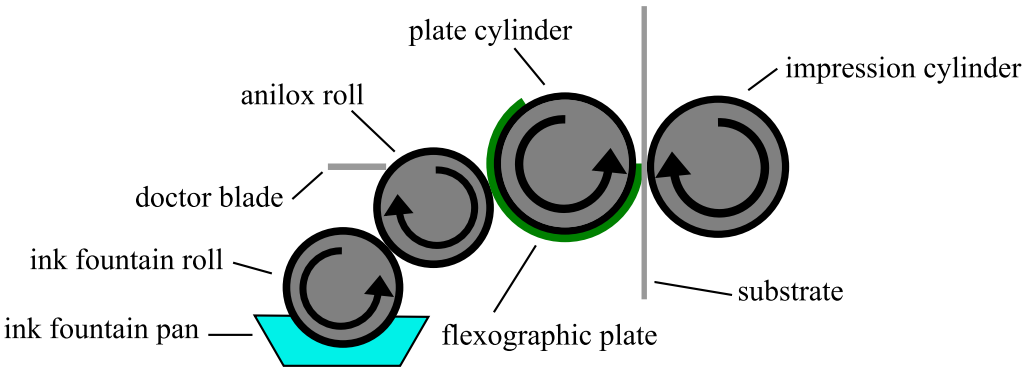

Figure 2.1. *Schematic diagram of a flexographic press. [3, p. 80]*

materials used in anilox manufacture. The surface of an anilox is covered by small holes called cells. During printing ink is transferred into these cells. The cells can be mechanically engraved but nowadays laser engraving is getting more and more popular. [3, p. 81; 4]

To achieve constant ink transfer, the anilox has to rotate smooth and steady. Rotational accuracy should be less than 0.01 mm and it is attained by firm anilox structure and careful fastening of anilox. [3, p. 81]

Biggest effect on the ink volume that anilox transfers to flexoplate is caused by the volume of the cells. Volume of an anilox is represented in units cm^3/m^2, so it describes how large volume of ink anilox can hold per surface area. Other factors that have an effect on the volume of ink transferred are the shape of the cells, the screen count of the anilox and the surface material of the anilox. [3]

There are several cell structures available. Those structures are trihelical, pyramid, quadrangular, hexagonal and hexagonal channel screen (figure 2.2) [4]. With laser engraving also circular cells can be made. The depth of the cell varies from 5 to 100 µm and the angle of the cell is usually 30, 45 or 60 degrees. [3, pp. 81–82]

Screen count describes how dense the cells are on the surface of the anilox. Unit of screen count is lines/cm (number of lines of cells per unit length). The screen count should be 2.5 to 4 times greater than the resolution of the picture. The smaller the value of the screen count, the larger the volume of the cells. Thus, more ink is transferred on the flexo plate but the printing resolution is lower. With large value of screen count the resolution of the picture can be higher, but the cell volume and the amount of ink transferred decreases. [3, p. 81]

Two types of anilox normally used are chrome and ceramic anilox. Chrome aniloxes are metal aniloxes with chrome coating. Thickness of the coating is from 10 to 30 µm. Chrome enhances the durability of the anilox and the life of a chrome anilox is about 30 to 50 million rounds. Disadvantage with chrome coating is that the coating reduces the cell volume and that during use the chrome coating often

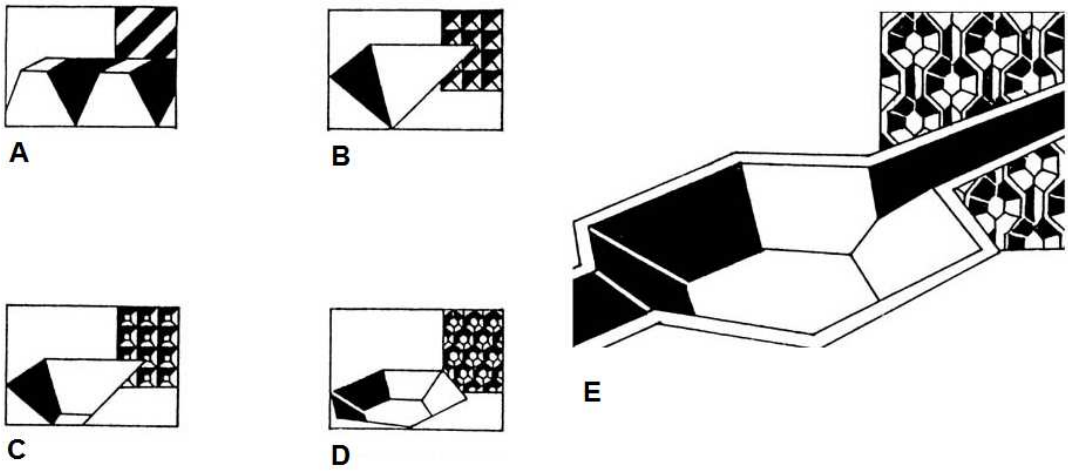

Figure 2.2. *Different anilox cell structures: A) trihelical, B) pyramid, C) quadrangular, D) hexagonal and E) hexagonal channel screen. [4]*

wears unevenly reducing the cell volume even more. Ceramic aniloxes are more wear-resistant and have lifetime of up to 10 times of that of chrome coated aniloxes, but they are also more expensive. [3, p. 81]

2.1.2 Doctor blade

Doctor blade ensures the constant amount of ink transfer from anilox to flexo plate by scraping excess ink off the anilox. Doctor blade is 0.1 - 0.2 mm thick and 2 - 5 cm wide strip of plastic, fibre glass or metal. Length of doctor blade depends on the width of the anilox it is used with. [3, p. 83]

Various factors have an effect on doctor blading quality. Such are the angle between doctor blade and the surface of anilox, the pressure between doctor blade and anilox, the shape of the blade, printing speed and ink viscosity. [3, p. 83]

2.1.3 Flexographic plate and plate cylinder

As was said earlier the flexographic printing plates are relief plates. This means that the printing areas (areas that transfer the ink to the substrate) are above the mean depth of the plate and the non-printing areas are below. [5, pp. 135–136]

The first flexible printing plates used in flexography were mould and made of rubber. Today rubber plates are still used but instead of moulding they are laser engraved. Another type of the flexo plates are the photopolymer plates. They are becoming more and more popular at the moment. These photopolymer plates are made by exposing the light sensitive polymer to ultraviolet (UV) light. Exposure to UV light initiates polymerization reaction that causes solidification of the polymer. Parts of the plate not exposed to UV light do not solidify and are washed away.

This leaves the wanted relief structure on the plate. The main benefits that have resulted from the introduction of photopolymer plates are improvement in printing resolution and decrease in the plate manufacturing time. [3, p. 77; 4]

Selection of the plates depends on the use of the plates and the ink used. For soft and rough substrates, such as cardboard, the plates are usually soft and thick. Since the plate softness reduces resolution, therefore harder and thinner plates are used when the surface properties of the substrates allow it. [3, p. 77] One must also pay attention on the solvents the ink contains when choosing the material of the printing plate. Some plates are non-resistant for some organic solvents and are therefore mostly used with water-based inks. Other plates can stand organic solvents better and can be used with many solvent-based inks. [6, 7]

Printing plates are attached to plate cylinder using double-sided tape. Plate cylinders are usually made of steel or aluminium. For fast and accurate printing process their rotational accuracy should be 0.05 mm or better. When bent around the plate cylinder, the outer face of the printing plate stretches in the tangential direction of the cylinder. This must be taken into account in plate making process. [3, p. 84]

2.1.4 Other parts

Fountain roll is a steel roll coated with natural or synthetic rubber. The coating must be resistant to the solvents used in the ink. The purpose of the fountain roll is to ensure constant supply of ink to the anilox. Speed of the fountain roll is slower than that of anilox, which improves the ink transfer to the anilox. [3, pp. 79–80; 4]

An alternative to fountain roll would be enclosed doctor blade system in which two doctor blades form a chamber where ink is pumped. Enclosed doctor blade system is widely used in newer flexographic presses. [3, p. 80]

Impression cylinder is smooth metal roll that supports the substrate when it contacts the printing plate. Speed of impression cylinder should be equal to that of plate cylinder. [4]

Flexographic press can consist of several different printing units and between the units there might be dryers that dry the ink. When printing with UV inks a UV light source is also needed to cure the inks. [3, pp. 84–85; 4]

2.2 Flexographic press used in this work

A full-scale flexographic press would be inconvenient to be used in research purposes. It would occupy large areas of valuable laboratory space and require large quantities of substrates and inks. For these reasons a laboratory scale flexographic press was used instead, despite the weaknesses it has. The flexographic press that was used

in this work was RK Flexiproof 100 from RK Print Coat Instruments Ltd.

2.2.1 RK Flexiproof 100

RK Flexiproof 100 is designed for testing inks and printing parameters on different substrates before the possible transfer to mass production. In research much smaller amounts of inks and substrates are used and therefore the structure and operation of RK Flexiproof 100 differ slightly from large-scale flexographic presses. Maybe the major difference is in the way the ink is applied on the anilox. As was seen in figure 2.1 the ink is normally applied by ink fountain or ink fountain roll. In RK Flexiproof 100 the amount of ink used is much smaller and is simply applied with a pipette straight on the anilox. For a test press this is probably a good and simple way to do it, because by doing so the amount of ink needed can be expressed in millilitres. This is fairly small amount when compared to large-scale presses that probably require litres of ink. Because formulated inks that are used in printed electronics are often quite expensive this saves lots of money. [8]

One problem that rises from the way the ink is supplied is that ink is open to evaporation, which can cause major change in the ink composition (concentration and viscosity will increase), especially when volatile solvents are involved. Solvent evaporation also causes the ink to dry on anilox thus clogging the small cells on its surface. Another problem that is faced with RK Flexiproof 100 is that anilox and plate and impression cylinders often do not have the rotational accuracy required. This causes uneven pressure distribution during printing process. The problems described above need to be taken into account, because they may cause the printing quality to appear worse than it would be when printing with a full-scale flexographic press.

The structure and major parts of RK Flexiproof 100 can be seen in figure 2.3. The apparatus number 21 is a UV light that is used to cure the UV inks. The press in our laboratory is not supplied with a UV lamp.

There are four parameters that can be adjusted in RK Flexiproof 100. Doctor blade pressure can be adjusted and it has effect on the amount of ink that is transferred to flexo plate. Anilox pressure is the pressure between anilox and plate roll. In RK Flexiproof 100 instead of value of pressure, the reading in the anilox pressure adjustment screw describes the distance between anilox roll and plate roll. One unit equals to 4 µm. Thus, the bigger the reading the smaller the pressure. Impression pressure adjustment works the same way. It controls the distance between plate cylinder and impression roll. One unit equals 4 µm. Also the printing speed can be adjusted in RK Flexiproof 100. It is done by the speed control. With RK Flexiproof 100 the printing speed can be chosen from 10 to 99 m/min. [8]

With RK Flexiproof 100 only single samples can be made. Usually after only one

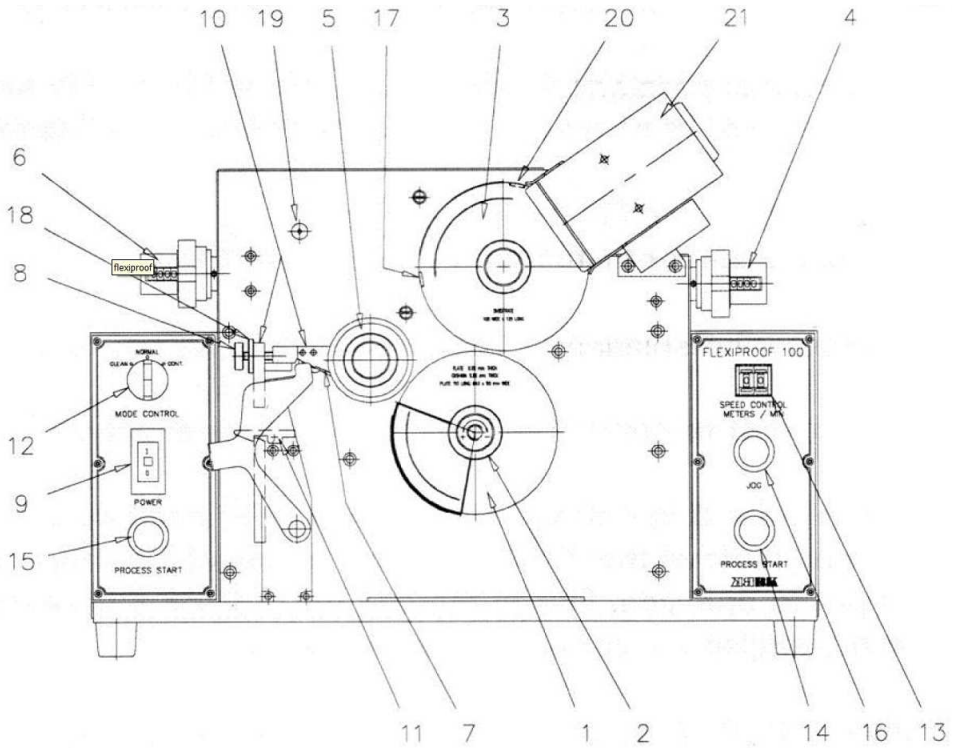

Figure 2.3. *Diagram of the flexographic press RK Flexiproof 100. Plate cylinder (1), impression cylinder (3), impression pressure adjustment screw (4), anilox roll (5), anilox pressure adjustment screw (6), doctor blade (7), doctor blade adjustment screw(8), power switch (9), doctor blade holder (10), mode control(12), speed control (13) and start button (14 and 15). [8]*

sample is printed, anilox, doctor blade and flexographic plate have to be cleaned or the printing quality collapses due to ink drying. Substrate size is limited to 297 mm × 105 mm (half the size of an A4 paper in lengthwise), but the actual printing area is even smaller (240 mm × 75 mm). During printing the substrate is attached to the impression roll. [8]

2.2.2 Flexographic plates used with RK Flexiproof 100

The plates used in this work were 1.7 mm thick photopolymer plates (figure 2.4). The yellow plate is a Miraclon BF plate, that has fairly good resistance for many organic solvents and the green plate is a ASAHI DSH plate that is suited for water and alcohol based inks. Both plates were ordered from Espoon Painolaatta Oy. [6, 7]

The printing pattern on the plates consists of two 30 × 30 mm squares that were used to print electrodes on substrates and bendy wires of different width that could be used for resistance measurements. In this work only the electrodes were used because poor printing quality did not allow the wires to be used in resistance

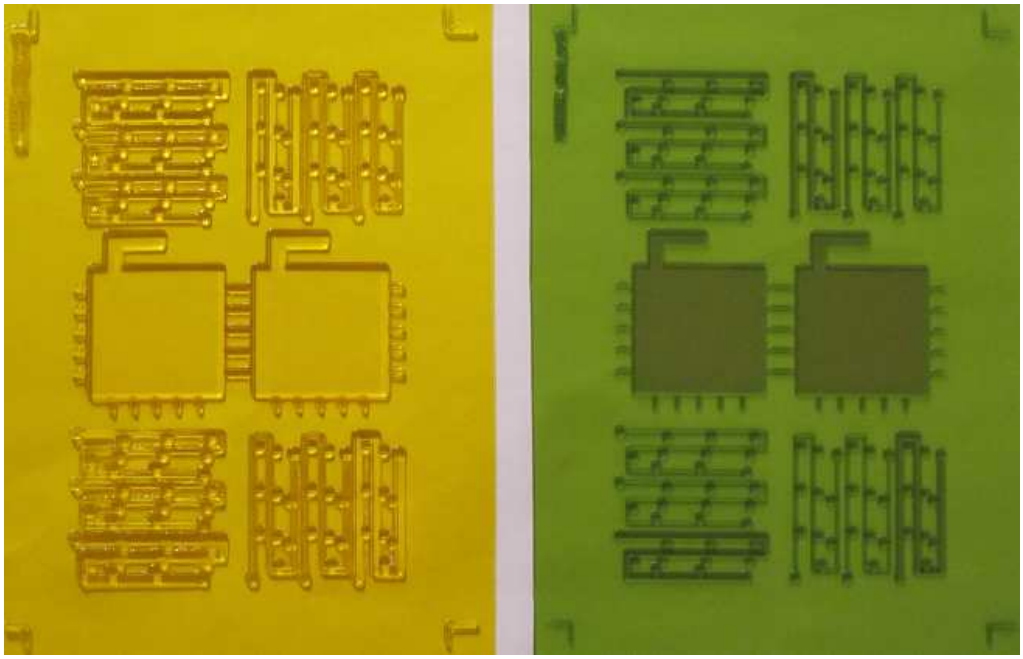

Figure 2.4. *Flexographic plates used in this work: Miraclon BF (yellow on the left) and ASAHI DSH (green on the right). Two big squares in the plates are used to print electrodes. Other structures are used to print structures for resistance measurements.*

measurements. Even though Miraclon BF can stand more solvent the ASAHI DSH plate was mostly used, because most inks that were used in this work were water based.

2.3 CX202 motorized bar coater

A good and fast way to test inks is depositing them on a substrate with CX202 motorized bar coater (a product of mtv messtechnik oHG) (figure 2.5). CX202 is a very simple apparatus and thus much faster and easier to use and clean than RK Flexiproof 100. It consists of main body, movable clamp for fastening up the substrate and moving bar holder for holding the bars that apply ink on the substrate.

The main body has control panel from which the speed and direction of the movement of the moving bar holder can be controlled. The speed of the bar holder can be set in a range from 10 to 100 mm/s with a control knob. The set speed is displayed in a digital display. On top of the main body there is a glass plate on which the substrate is fastened up during the ink deposition.

The movable clamp has a locking handle, which is used to lock the movable clamp at a certain position. The more to the right the clamp is locked the shorter is the distance that the bar holder travels. Substrate is fastened between the clamp and the glass plate by a clamping screw that is on top of the clamp.

The moving bar holder can be equipped with several accessory equipments. In

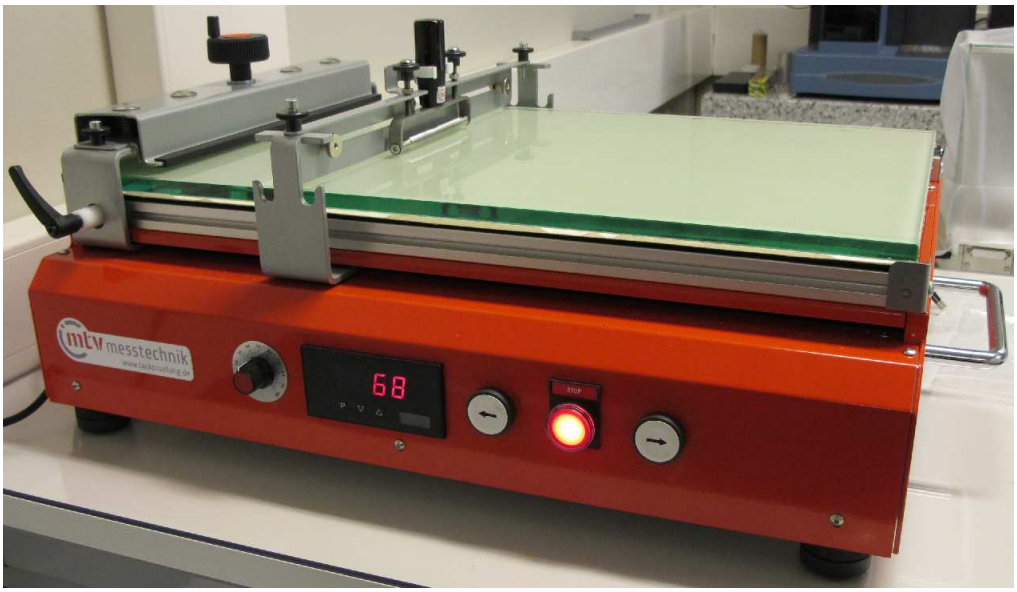

Figure 2.5. *CX202 motorized bar coater that was used for ink testing in this work.*

this work the accessory equipment used was a BG profile bar coater that consists of a screw profile bar and a handle for the bar. The bar is attached to the handle with two screws and the handle with the bar is then attached to a clamp at the moving bar holder. Contact and adequate pressure between the bar and the substrate are adjusted with two adjusting screws. Various bars of different width for various wet film thicknesses are available. The ones used in this work were for applying 4, 6, 10 and 12 µm thick and maximum of 80 mm wide wet films. The thickness of dry film depends on the ink used.

Although the CX202 is a handy apparatus, certain caution must be used with the results derived from the samples made with it. A good and uniform film achieved with CX202 does not necessarily mean that as good results can be achieved with RK Flexiproof 100 and therefore further investigation is needed to find out the flexographic printability of that ink. On the other hand from a poor result got with CX202 one can be sure it is not going to work with RK Flexiproof 100 either and thus save a lot of time and effort.

One problem that was faced with CX202 was uneven rolling of the screw profile bar. This was due to poor attaching mechanism of the bar, which caused occasionally the bar to stop rolling. This further led to uneven ink application and film thickness.

3. INTERFACIAL PHENOMENA

Interfaces are everywhere, and the phenomena that take place at interfaces have major effect in our everyday life. In many cases the phenomena at the interface are so remarkable that they definitely have to be taken into account when inspecting a system of multiple phases and not just the properties of the bulk phases. In this work the interfaces are the ones between ink, substrate and air. Together with ink viscosity, interfacial forces have major effect on printing quality. [9, pp. 1–2]

3.1 Surface tension

Surface tension is responsible for the water droplets to be spherical and for water striders (an insect) to walk on the surface of water. If a two-phase system, containing liquid and gas phases, is examined one can understand better the fundamentals of surface tension.

When reaching to the gas phase from the bulk liquid phase a major decrease in concentration and density will take place within a very short distance at the interface. For water, for example, this change is more than thousand fold. Figure 3.1 illustrates this change. In bulk liquid phase the distance between molecules is much shorter than in gas phase. Due to the shorter distance also attractive cohesive forces between alike molecules are much greater in bulk liquid phase than in gas phase. [9, pp. 2–10]

As can be seen in figure 3.2 the molecules in bulk liquid phase experience attractive forces from all directions, resulting in zero net force. However, this is not the case for the molecules positioned at surface of the liquid phase. The surface molecules have alike molecules next to them on side and below, but above at the gas phase the molecules are further away thus resulting in smaller attractive force from above. This leads to unbalanced net force that tries to "pull" surface molecules into the bulk liquid phase. This force is called the surface tension and is responsible for the round shape of water droplets. Surface tension is the force per unit length acting on an imaginary line drawn in the surface as can be seen in following equation

$$\gamma = \frac{F}{\delta x}, \tag{3.1}$$

where γ is the surface tension and F is the force acting tangentially to the surface and at right angles to an element, δx, of an imaginary line in the surface. [9, pp.

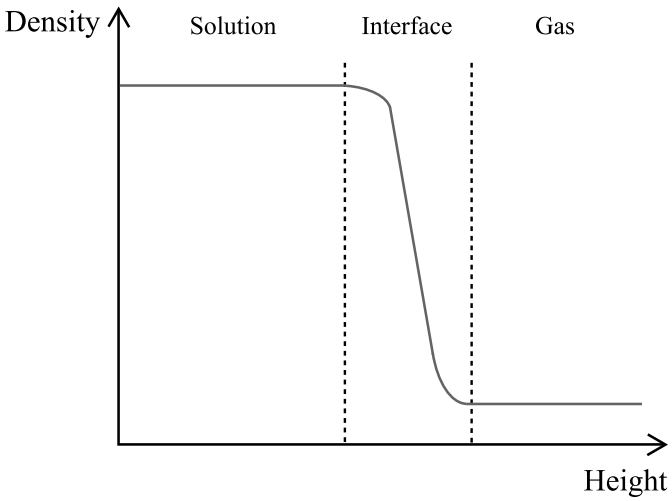

Figure 3.1. *The change in density, when arriving from bulk liquid phase to gas phase. [9]*

8–10]

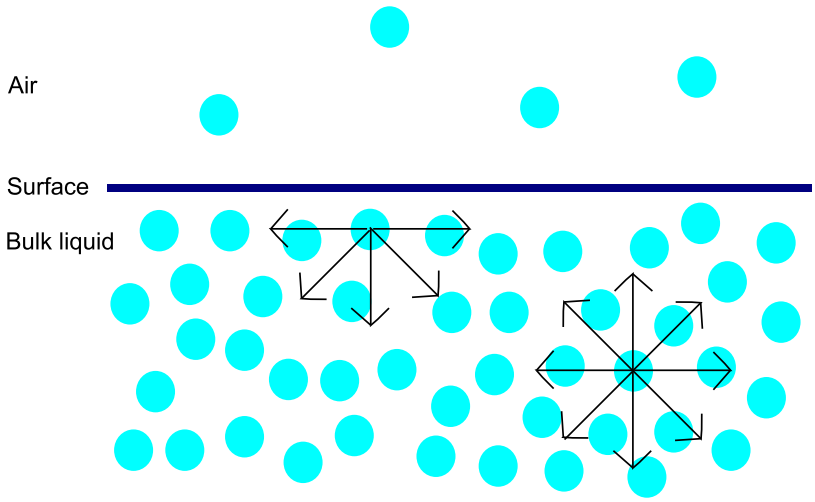

Figure 3.2. *Forces acting on molecules near surface and in bulk liquid. [9, p. 3]*

3.2 Contact angle

When a drop of liquid is deposited on a solid surface a triple interface between solid, liquid and gas is formed (figure 3.3). The shape of the drop depends on the magnitude of interfacial tensions acting on the triple interface. In equilibrium the interfacial tensions are in balance and the situation can be described by following equation

$$\gamma_{GS} = \gamma_{LS} + \gamma_{GL} \cos\theta, \tag{3.2}$$

where γ_{GS}, γ_{LS} and γ_{GL} are the interfacial tensions of gas-solid, liquid-solid and gas-liquid interfaces respectively. The angle θ is the contact angle that is the angle between solid surface and the tangent to the liquid surface at the line of contact with the solid. [9, p. 11]

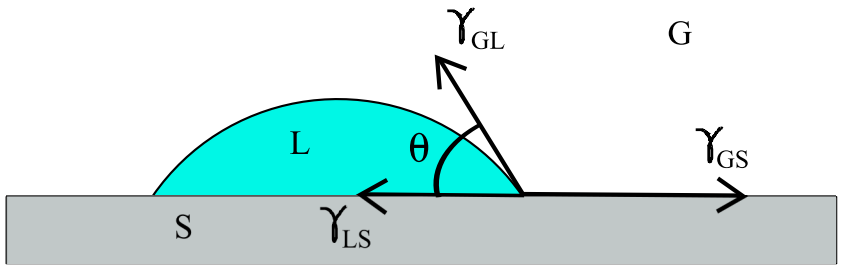

Figure 3.3. *Contact angle. [9, p. 11]*

The interfacial tensions depend greatly on the nature of the substances at the interface. A water droplet is fairly spherical and has large contact angle on hydrophobic surfaces whereas on hydrophilic surface the contact angle is small and the droplet spreads on the surface. Term wetting is used to describe how a liquid behaves on a surface. If the $\theta < 90$ the liquid wets the surface. If $\theta = 0$ the wetting is complete. When $\theta > 90$ the liquid does not wet the solid surface. [9, pp. 11–12]

The contact angle between ink and substrate has to be adjusted at certain value in order to obtain required printing quality. In flexographic printing with water-based inks (as was the case for most of the inks in this work) on polymer substrates the problem is usually too high contact angle due to the high surface tension of water and low surface energy of the substrate. One way to lower the contact angle is to lower the surface tension of these inks by adding low-surface tension solvents or surfactants into the ink. Another way to affect the value of contact angle is to tune the surface energy of the substrate.

Ink properties on certain substrate can be studied by measuring the contact angle between the substrate and ink with a contact angle-measuring instrument. In this work some contact angle measurements were made using Krüss DSA30. For relatively large contact angles this instrument appeared quite useful, but major problems occurred when measuring smaller contact angles (as is the case between formulated, low surface tension inks and substrates). Therefore the only contact angles that are represented in this thesis are the ones that were measured between distilled water and PET or PVDF substrates (section 7.2).

3.3 Surfactants

Surface-active agents or surfactants are amphiphilic molecules, which means that one end of the molecule is hydrophobic (water insoluble = oil soluble) and the other

end is hydrophilic (water soluble). Surfactants can be anionic, cationic or non-ionic. In this work only an anionic surfactant was used. [9, pp. 56–57]

Anionic surfactants like sodium dodecyl sulfate (SDS) (used in this work) consist of a long hydrophobic hydrocarbon chain (tail) and an anionic head (figure 3.4). This kind of surfactants are often used in detergents, where their hydrophobic tails attach to grease stain and the hydrophilic heads help to dissolve the grease into water. [9] In printed electronics surfactants are not used to dissolve grease, but to lower the surface tension of (water-based) inks, making them more printable.

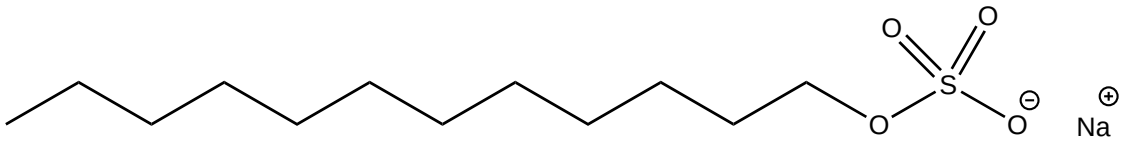

Figure 3.4. *The structure of a SDS molecule. [9]*

In addition to the property of decreasing ink's surface energy, SDS can improve the dispersebility of the conducting components into solvent used in ink as well as the conductivity of the printed structure. These additional properties of SDS will be further discussed in chapter 6.

3.4 Cohesion and adhesion

In a multiphase system both cohesion and adhesion take place. Cohesion is the interaction between like molecules and adhesion is the interaction between different molecules. In printable electronics adhesion describes the strength of the interface between substrate and printed material. Cohesion describes the strength that holds the molecules of printed material together. [10]

Accurate and reliable testing of adhesion and cohesion is difficult. One method to test adhesion is a tape test in which a special tape is pressed against the printed ink film and then torn away. The more ink stays at the substrate the better the adhesion. [11]

4. ELECTRICAL MEASUREMENTS

When making conducting electrodes that are needed for the pressure sensors manufactured in this work, the electrical properties of the electrodes have to be controlled and characterized. Sheet resistance is a generally used magnitude to describe the electrical properties of these electrodes. It can be measured quite accurately by using four-point measurement.

4.1 Sheet resistance

When the electrical properties of a thin film are measured, conductivity (or resistivity) of the electrode material may not be the most useful value to be measured. Instead, sheet resistance, which does not take the film thickness into account, is a useful tool to describe the electrical properties of a thin film. Sheet resistance can be derived starting from following equation, which describes the resistance of a conductor

$$R = \rho \frac{L}{A}, \tag{4.1}$$

where ρ is the resistivity of the material, L and A are the length and cross sectional area of the conductor respectively. Usually equation 4.1 is used to calculate the resistance of a wire, but if instead we think it to be a thin rectangular film (figure 4.1), and replace the cross sectional area A with the product of thickness t and width W of the film, we get equation

$$R = \rho \frac{L}{Wt}, \tag{4.2}$$

from which after a small rearrangement we further get equation

$$R = \frac{\rho}{t} \frac{L}{W} = R_S \frac{L}{W}, \tag{4.3}$$

where R_S is sheet resistance. [12, 13] As can be seen from equation 4.3, sheet resistance should have the same unit, Ω, as resistance has. To distinguish these two from each other, for sheet resistance unit ohms/square (Ω/□ or Ω/sq) is often used. For a square shaped ($W = L$) film of constant thickness t (figure 4.1), the value of R_S stays constant regardless of the square dimensions. [13]

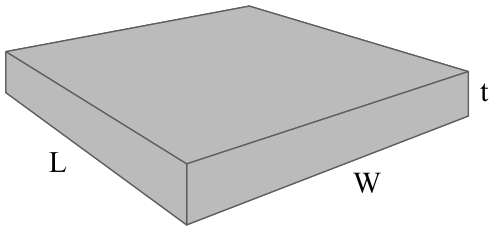

Figure 4.1. *A rectangular thin film sample of length L, width W and thickness t.*

4.2 Four-point measurement

Normally, when one wants to measure the resistance of a sample or device, one simply takes a multimeter, puts it on resistance measuring mode, makes contact to the sample with the two probes, and then reads the reading from meter's display. This method, called two-point measurement, gives a result that is accurate enough as long as the resistance of the device under test (DUT) is high compared to contact resistances.

In two-point measurement each contact to the sample serves as a current and as a voltage probe. The reading in the multimeter is the total resistance of the circuit, not just the resistance of DUT as can be seen in following equation

$$R_T = \frac{V}{I} = 2R_W + 2R_C + R_{DUT}, \tag{4.4}$$

where R_T is the total total resistance of the circuit, R_W is the wire or probe resistance, R_C is the contact resistance between the probe and the device and R_{DUT} is the resistance of DUT. The value of R_{DUT} cannot be distinguished from equation 4.4 since the values of R_W and R_C are not known. [14]

To overcome the problem that is faced with two-point measurement, two more probes have to be added into the measurement setup. This new setup is called four-point measurement since it has four probes. One way to measure the R_S from large area film is to use four probes in line with equal spacing (figure 4.2) [15]. In this setup the two outermost probes are used to apply current through the sample or device, while the two innermost probes are used to measure the voltage. This improved setup does not exterminate the parasitic resistance caused by R_W and R_C but when a high impedance (10^{12} Ω or higher) voltmeter is used the effect of these parasitic resistances becomes negligible when compared to the total resistance of the inner circuit. [14]

If the setup in figure 4.2 is used to measure infinitely large sample ($a = b = \infty$) of thickness much smaller than the spacing of the probes ($t \ll s$), the sheet resistance is as follows

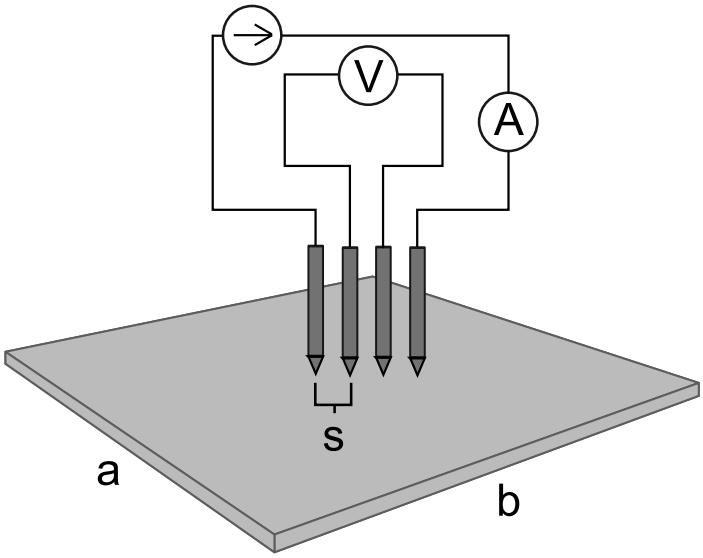

Figure 4.2. *Four probe measurement setup that is used to measure sheet resistance for thin film samples.*

$$R_S = \frac{\pi}{\ln 2}\frac{V}{I} \approx 4.5324\frac{V}{I}, \tag{4.5}$$

where I is the current between the two outermost probes and V is the voltage measured between the two innermost probes. $\pi/\ln 2$ is a geometric factor for infinitely large sample. Because equation 4.5 is valid only for very large samples, more corrections have to be made when smaller samples are measured. For finite size rectangular shape sample correction factor depends on the dimensions a and b of the sample as well as the shape (ratio of the length and width) of the rectangle. Also the ratio of dimensions and probe tip spacing has an effect that has to be taken into account. Now the corrected value for the sheet resistance for finite size rectangular sample is

$$R_S = G\frac{\pi}{\ln 2}\frac{V}{I} \approx 4.5324G\frac{V}{I}, \tag{4.6}$$

where G is the additional geometric correction factor that depends on the dimensions and shape of the sample. Values of G for samples of different size and shape can be found in table 4.1. From the table clearly can be seen that the smaller the sample gets, the larger corrections have to be made. With tip spacing the case is the opposite. The smaller the tip spacing gets, the less correction has to be made. That is why probe tips should not be too far apart from each other, especially when measuring fairly small samples. [15]

Table 4.1. *Geometric correction factors G for 4-probe sheet resistance measurement for finite size rectangular shape thin film sample. [15]*

b/s	$G(a/b=1)$	$G(a/b=2)$	$G(a/b=3)$	$G(a/b\geq 4)$
1			0.2204	0.2205
1.25			0.2751	0.2751
1.5		0.3263	0.3286	0.3286
1.75		0.3794	0.3803	0.3803
2		0.4292	0.4297	0.4297
2.5		0.5192	0.5194	0.5194
3	0.5422	0.5957	0.5958	0.5958
4	0.6870	0.7115	0.7115	0.7115
5	0.7744	0.7887	0.7888	0.7888
7.5	0.8846	0.8905	0.8905	0.8905
10	0.9313	0.9345	0.9345	0.9345
15	0.9682	0.9696	0.9696	0.9696
20	0.9822	0.9830	0.9830	0.9830
40	0.9955	0.9957	0.9957	0.9957
∞	1	1	1	1

4.3 Keithley 2425 100 W SourceMeter and four-point probe

As was said earlier, four-point measurement ensures precise measurement of sheet resistance. The sheet resistance measurements done for this thesis were carried out with Keithley 2425 100 W SourceMeter (figure 4.3 A)) which is both highly stable direct current (DC) power source and a true instrument-grade $5\frac{1}{2}$-digit multimeter, so no external voltmeter is needed for four-point measurements. [16]

Keithley 2425 is capable of driving 100 V voltage and 3 A current. These limiting values suit more than well the requirements for sheet resistance measurements done in this work. It would be possible to use Keithley 2425 as an ohmmeter and directly measure the resistance of the sample, but if the sample is a thin electrode, as it is in this case, that kind of measurement would not give the value of sheet resistance directly. Instead, source current was set at desired value and the voltage was measured (figure 4.2). Sheet resistance was then calculated by using equation 4.6. Keithley 2425 is also capable of doing computer programmed current sweep measurements (MATLAB for example). [16]

To make further evaluation of sheet resistance easier, equation 4.6 shows that if the source current applied into the sample is selected to be $4.5324 \cdot 10^x$A, $x \in \mathbb{Z}$ the

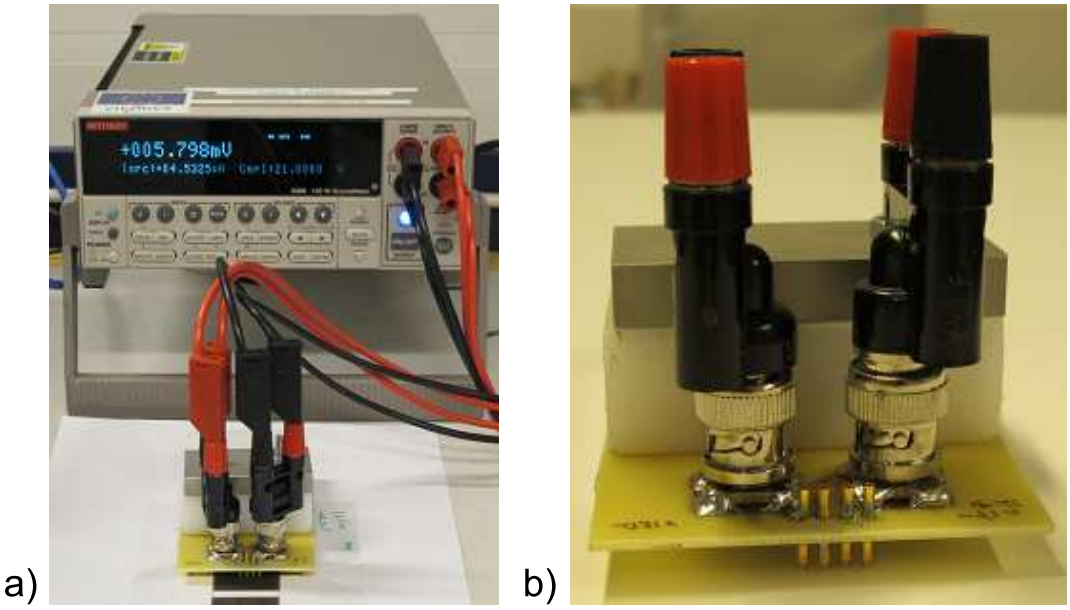

Figure 4.3. *a) Keithley 2425 100 W SourceMeter with four-point probe connected measuring sheet resistance of an electrode printed on PVDF substrate and b) a close-up view of four-point probe.*

reading of the voltage in volts is the value of sheet resistance (before the geometric correction from table 4.1) in ohms/sq times 10^{-x}.

The four-point probe (figure 4.3 B)) used to measure the sheet resistances of the electrodes is a simple self-made apparatus. Contact to the sample is made by four spring contact probes. The model of spring contact probes is Feinmetall F620, purchased from Farnell. They are gold plated, have working travel of 1.3 mm and tip diameter of 1.2 mm. At working travel the spring force is 75 cN. Spring contact probes spread the load evenly on all four probes, which prevents damage to the sample and makes the contact even. [17]

The four-point probe is assembled on a printed circuit board (PCB). The four spring contact probes are soldered in a line with 3 mm tip spacing at the edge of the PCB. Two BNC connectors are soldered on topside of PCB. One of them is used to apply current through the sample and the other is in contact to the two innermost probes that measure the voltage. BNC - banana connector adapters and measuring wires were used to make contact between four-point probe and Keithley 2425. To ensure adequate pressure and contact during measurements an additional metal weight was added to the four-point probe.

5. PIEZOELECTRICITY

In 1880 the famous French brothers Pierre and Jacques Curie discovered that in some crystals, such as quartz, topaz, tourmaline, Rochelle salt and cane sugar an electric charge is developed on certain parts of the surface when exposed to mechanical stress. The phenomenon was named piezoelectricity after a Greek word 'piezin' which means to press. Piezoelectricity is closely related to pyroelectricity, a phenomenon that develops electric charge on certain crystals when a change in temperature occurs. In fact, all pyroelectric materials also exhibit piezoelectricity. Pierre Curie's previous work on pyroelectricity and symmetry of crystals had an influence on his and Jacques approach to piezoelectricity. Since the discovery, numerous applications based on piezoelectricity have been invented. [18, p. 103; 19, pp. 17–19; 20, pp. 10–11]

In order for a material to exhibit piezoelectricity, it has to show non-centrosymmetric crystallinity. Of the 32 point groups into which all crystalline materials may be categorized, 11 are centrosymmetric. Of the remaining 21 point groups 20 are piezoelectric and only 10 are pyroelectric. Both natural (quartz, tourmaline, cane sugar) and man-made (polyvinylidene fluoride (PVDF), lead zirconate titanoate (PZT)) piezoelectric materials exist. [21]

5.1 Piezoelectric effect

Piezoelectricity is a cross coupling effect between the elastic variables (X stress, x strain) and the dielectric variables (D dielectric displacement, E electric field). The partial differentials of these variables define constants d, e, g and h

$$d = \left(\frac{\partial D}{\partial X}\right)_E = \left(\frac{\partial x}{\partial E}\right)_X \tag{5.1}$$

$$e = \left(\frac{\partial D}{\partial x}\right)_E = -\left(\frac{\partial X}{\partial E}\right)_x \tag{5.2}$$

$$g = -\left(\frac{\partial E}{\partial X}\right)_D = \left(\frac{\partial x}{\partial D}\right)_X \tag{5.3}$$

$$h = -\left(\frac{\partial E}{\partial x}\right)_D = -\left(\frac{\partial X}{\partial D}\right)_x \tag{5.4}$$

In equations 5.1 - 5.4 the first definition refers to the direct piezoelectric effect and

the second one to the converse piezoelectric effect. [22]

Constants d and g (equations 5.1 and 5.3) are the most commonly used constants to describe the properties of a piezoelectric material. Subscripts are used to further fix the constants to certain axes of the crystal. The first number refers to the electrical axis while the second number refers to the mechanical axis [23]. In general, coefficient d can be written as a 3×6 matrix

$$d_{ij} = \begin{bmatrix} d_{11} & d_{12} & d_{13} & d_{14} & d_{15} & d_{16} \\ d_{21} & d_{22} & d_{23} & d_{24} & d_{25} & d_{26} \\ d_{31} & d_{32} & d_{33} & d_{34} & d_{35} & d_{36} \end{bmatrix} \tag{5.5}$$

where 1, 2 and 3 refer to the three major axes (x, y and z) of a piezoelectric material and 4, 5 and 6 represent the shear about these axes respectively. [24]

5.1.1 Direct piezoelectric effect

Direct piezoelectric effect was the first effect that the Curie brothers discovered in 1880. In direct piezoelectric effect when a piezoelectric material is pressed or stretched, dipoles in the material move and form a charge or potential difference on two opposing surface of the material (figure 5.1).

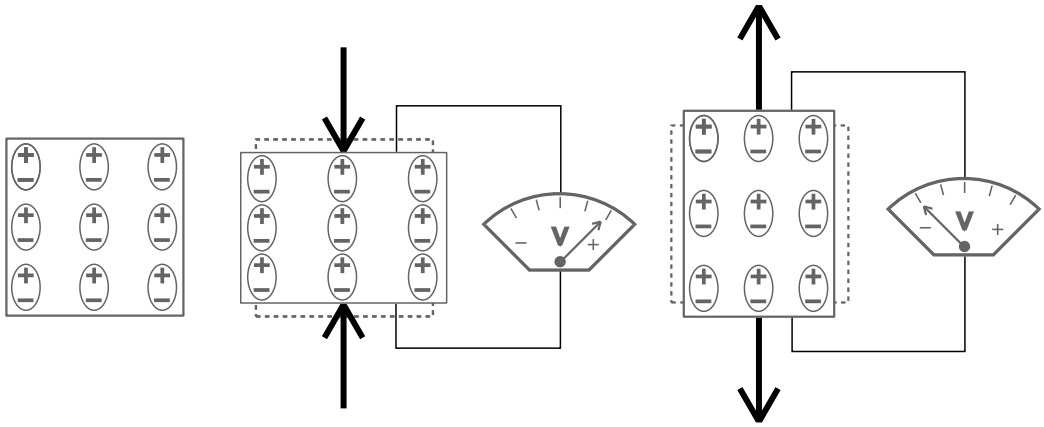

Figure 5.1. *Direct piezoelectric effect. A voltage (or charge) difference will form on different sides of piezoelectric material when a force is applied to it. [20, p. 13]*

Direct piezoelectric effect is the foundation for many sensor applications, such as pressure, force and acceleration sensors. The charge distribution caused by the stress is not permanent and thus with piezoelectrics only dynamic and not static forces can be measured. Most materials allow fairly low frequency measurements, though.

5.1.2 Converse piezoelectric effect

Converse piezoelectric effect is the opposite effect for direct piezoelectric effect. In other words, when an external electric field is applied to a piezoelectric material, it forces the dipoles to move and thus stretches or contracts the material depending on the direction of the applied field. The converse effect was discovered soon after the direct effect.

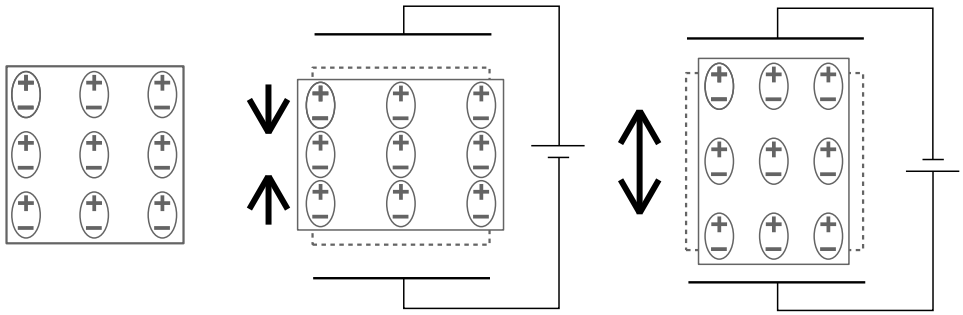

Figure 5.2. *Converse piezoelectric effect. External electric field will stretch or contract a piezoelectric material, depending on the direction of the applied field. [20, p. 13]*

Applications in which converse piezoelectric effect can be exploited are sonar, piezoelectric speaker and electromechanical transducers. An electromechanical transducer is a device that converts electricity into mechanical energy.

5.2 Polyvinylidene fluoride (PVDF)

Polyvinylidene fluoride, or PVDF is a semicrystalline fluoropolymer having crystallinity of 50 to 60 %. At least four crystal phases, named α, β, γ and δ exist in PVDF. [25] The manufacture of PVDF is done by polymerizing vinylidene fluoride monomer ($C_2H_2F_2$). The polymerization reaction results in polymer structure that has repeating unit which consist of two carbon atoms, one with two hydrogen atoms attached to it and one with two fluoride atoms attached to it (figure 5.3).

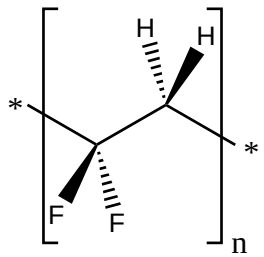

Figure 5.3. *The structure of the repeating unit in polyvinylidene fluoride, PVDF.*

PVDF is a chemically inert polymer and has very good mechanical properties. It is therefore used in various applications in harsh conditions, such as valves, tanks and piping systems in the chemical processing industry. In addition to chemical and mechanical toughness, PVDF has one unique property in the world of polymers. It shows remarkable piezoelectricity when stretched and poled to form crystal β phase.

5.2.1 Piezoelectricity in PVDF

Piezoelectricity in PVDF was first discovered by Japanese scientist Heiji Kawai in 1969. The strong piezoelectricity that poled PVDF shows, rises from its strong dipole moment. Fluorine atom is very small, having van der Waals radius of only 1.35 angstroms that is comparable to that of hydrogen's 1.2 Å. In PVDF fluorine atoms form highly polar bonds with carbon atoms. Dipole moment of a fluorine carbon bond is $\mu = 6.4 \cdot 10^{-30}$ Cm. [26]

In order to make PVDF film piezoelectric couple of stages have to be gone through. First, PVDF film is annealed and stretched uni- or biaxially. Temperature for this stage can be up to 150 °C. Second, the stretched film is poled by using a strong electric field of up to 140 MV/m. Poling lasts about an hour and the temperature is kept at an elevated level. After poling the film is cooled down, maintaining the poling electric field. During stretching and poling the non-piezoelectric α phase of PVDF turns into piezoelectric β phase (figure 5.4). [27, pp. 5-50–5-51]

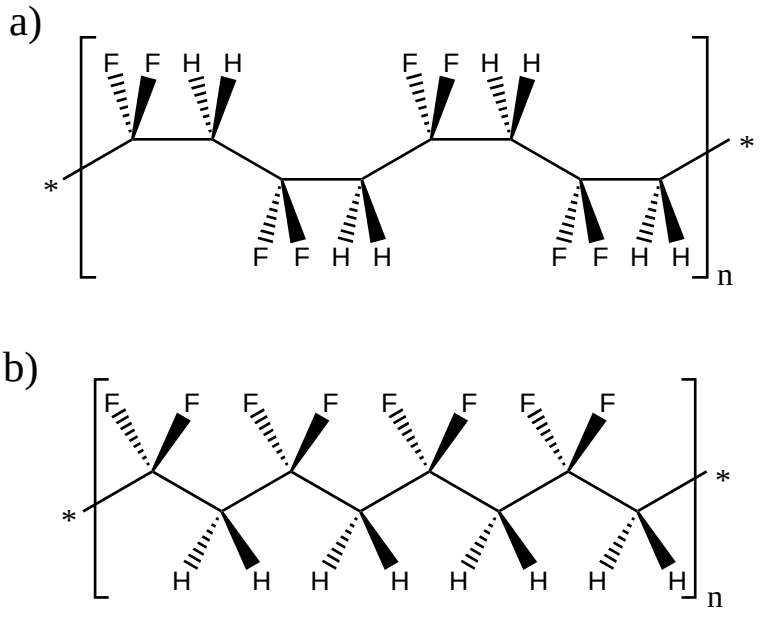

Figure 5.4. *Structures of a) non-piezoelectric α phase and b) piezoelectric β phase PVDF. [27, p. 5-50]*

In this work uniaxially stretched and poled β phase of PVDF substrate was used. The β phase of PVDF is orthorombic C_{2v} (mm2) [21, 28] and due to its crystal symmetry the number of independent piezoelectric coefficient is reduced and d can be represented as following matrix.

$$d_{ij} = \begin{bmatrix} 0 & 0 & 0 & 0 & d_{15} & 0 \\ 0 & 0 & 0 & d_{24} & 0 & 0 \\ d_{31} & d_{32} & d_{33} & 0 & 0 & 0 \end{bmatrix} \tag{5.6}$$

For uniaxially stretched PVDF film the axis 1 is in the direction of stretching, axis 2 is normal to the stretching direction in the plane of the film and axis 3 is normal to the plane of the film [28]. Because in this work PVDF film was used as pressure sensor only coefficient d_{33} is of interest since the pressure is normal to the plane and the electrodes are printed on the surface of the film. However the aim on the future work is to use similar sensor elements for measuring also the shear stresses which are required for shoe sensor application [2]. In table 5.1 the properties of the film used in this work are represented.

Table 5.1. *Properties of piezoelectric PVDF used in this work. [23]*

Symbol	Parameter	Value	Unit
t	Thickness	9, 28, 52, 110	10^{-6} m
d_{31}	Piezo Strain Constant	23	10^{-12} C/N
d_{33}	Piezo Strain Constant	-33	10^{-12} C/N
g_{31}	Piezo Stress Constant	216	10^{-3} m^2/C
g_{33}	Piezo Stress Constant	-330	10^{-3} m^2/C
C	Capacitance	380 for $28 \cdot 10^{-6}$ m film	pF/cm^2 @ 1 kHz
ϵ/ϵ_0	Relative Permittivity	12-13	
ρ	Density	1.78	10^3 kg/m^3
	Temperature Range	-40 to 80...100	°C

5.2.2 Piezoelectric PVDF pressure sensor

Because of its flexibility, small thickness and strong piezoelectricity, one useful application for PVDF is as material for pressure sensors. To make a pressure sensor from PVDF film conducting electrodes have to be applied on both sides of the PVDF film in order to collect and transfer the charge, that is build up due to the applied pressure, to a measurement unit. The electrodes can be deposited with various methods and they can be made of various materials as will be discussed later in chapter 7. In this work main focus was in electrodes that were printed with flexography.

There are available some commercial piezoelectric pressure sensors made of PVDF. One of the major manufacturers of these sensors is Measurement Specialties. They offer sensors that have either sputtered NiCu or screen printed silver electrodes. Those sensors are small and rectangles in shape. The electrodes that are printed with RK Flexiproof 100 in this work are squares of 3 cm by 3 cm in size. Those electrodes have also L- or I-shaped extensions to make it easier to connect them into measurement unit. Figure 5.5 illustrates the newest structure of the electrodes printed in this work. Older plate design have I-shaped extensions.

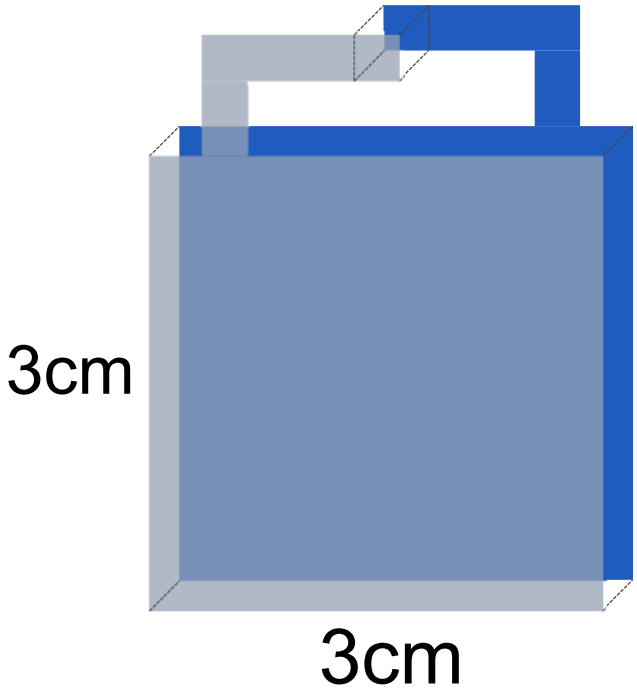

Figure 5.5. *The newest structure of flexoprinted piezoelectric pressure sensors that were fabricated in this work.*

Sensitivity is one of the most important properties of a piezoelectric sensor. With sensitivity measurements values of piezoelectric constant d (equation 5.1) can be measured. The bigger value of d is achieved the more sensitive the sensor is and the smaller forces or pressures it can measure. The measuring equipment used to measure sensitivities in this work was assembled and operated by our collaborator Ville Rantanen [29].

5.3 Sensitivity measurement setup

A Brüel & Kjaer Mini-Shaker Type 4810 (figure 5.6) was used to apply dynamic excitation force to the samples. 2 Hz sinusoidal signal generated by a function generator was used to control the shaker's 4 mm of diameter piston that presses the sample against a metal plate. Samples were kept in place during the measurement

by applying a static force of approximately 3 N between the sample and the shaker's piston. The static force was adjusted by position adjustment screw. A commercial dynamic force sensor (PCB Piezotronics model 209C02) was used to measure the dynamic force applied to the sample.

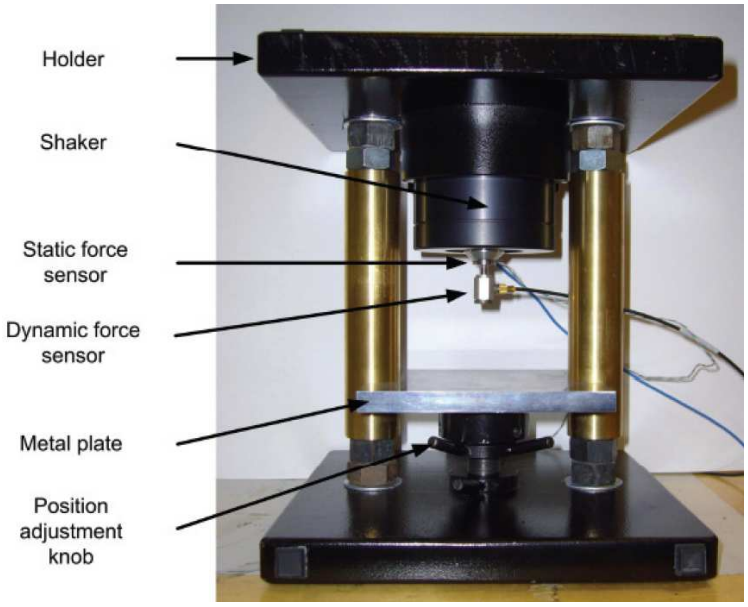

Figure 5.6. *Brüel & Kjaer Mini-Shaker Type 4810 that was used in the sensitivity measurements [2]*

Electric contacts to the samples were made by using alligator clips or pieces of circuit board. Contacts were made to the extensions that stick out of the electrode. If the sample had no extensions, contacts were made at the edge of the electrode. Some difficulties appeared in making good electrical contacts to the electrodes, which may affect the results of sensitivity measurements (chapter 8.2).

To avoid short-circuiting the two electrodes on opposite sides of the samples, a piece of overhead transparency was used as an insulator on one side of the sample, when contacts were made to the sample. Pieces of overhead transparencies were also used on both sides of the samples to protect and insulate the electrodes from the shaker's piston. This also simplified the handling of the thin PVDF film by making it less flexible.

Both signals, the one from the dynamic force sensor and the one from the sample, were input to a 2.5 V student-use designed analog-to-digital converter (ADC). The ADC has 4 channels with charge amplifiers and 4 channels that measure voltage. Channels with charge amplifiers were calibrated by inputting a sinusoidal signal through a 10 nF reference capacitor, and resolving the amplification. Channels that measured voltage were calibrated by inputting a sinusoidal signal and resolving the amplification.

Baseline corrections were made to the charge signals received from the PVDF samples and a sine curve was fit to them for further calculations. The sine curves had good fit for most of the samples. Peak-to-peak values for the dynamic force measurements were approximately 1.3 N, meaning that the force applied to the sample had a approximate range from 2.35 to 3.65 N, 3 N being the average force applied to the sample.

6. CONDUCTING INKS

In printable electronics electronic components are printed by using inks with different electrical properties. Inks can be conducting, semi-conducting or dielectric. Conducting inks are used for printing wires, electrodes etc. Semi-conducting inks are used in active components such as transistors and diodes. In this work inks with different materials are studied in order to fabricate conducting electrodes. [1]

To print conductors on a substrate, conducting inks are needed. There are a wide variety of commercial conducting inks on the market and one can also formulate them on one's own. What makes ink suitable for a particular application depends on many variables. Just to mention some: cost, viscosity, surface tension, sintering temperature (for metal inks), toxicity etc.

For this thesis a few different type of inks were used. Some formulated inks are based on carbon nanotubes, some on conducting polymer (PEDOT:PSS) and some are silver flake inks. The nature and structure of those inks differ greatly from each other, but they all show at least moderate conductivity.

6.1 CNT inks

The functionality of carbon nanotube (CNT) inks are based on unique properties of CNTs. CNTs are one allotropic form of carbon, just like diamond and graphite. Discovery of CNTs was done at the latest by Sumio Iijima in 1991 [30], but there are evidences that CNTs were already found in the early 1950's [31]. Manufacture of CNT solutions for CNT ink is very challenging because CNTs tend to agglomerate from the solution.

6.1.1 Chemistry of carbon

Although carbon atom has only six electrons and is therefore one of the simplest atoms, its structure is unique, enabling the formation of very complex molecules. Carbon is found in all living organisms, where it is the main building block of many molecules. Pure carbon can exist in five allotropic forms: graphite, diamond, fullerene, graphene and carbon nanotube.

The electrons in a single carbon atom in its ground state have distributed as follows: two in the 1s orbital, two in the 2s orbital, one in the $2p_x$ orbital and one in the $2p_y$ orbital (figure 6.1). From this configuration we would not assume the

tetravalent bonding peculiar to carbon, rather bivalent or trivalent bonding [32, p. 29]. However, in molecules that carbon is present it occurs as a tetravalent atom, having four valence electrons for bond forming. This tetravalent character can be described so that in crystalline phase the carbon atom is in excited state, where one of the electrons from 2s orbital has shifted up to $2p_z$ orbital (Figure 6.1) [33, p. 5]. When in molecular form, the carbon orbital hybridization has to be considered.

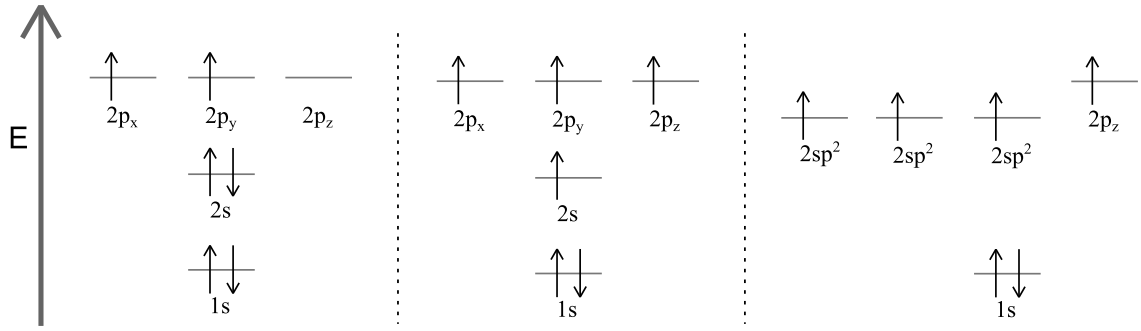

Figure 6.1. *Electron configuration of a carbon atom on ground state (left) and on excited state (middle). $2sp^2$ hybridization, found in graphite, graphene and CNTs is represented on the right.*

In hybridization the 2s and one to three of the 2p orbitals are hybridized resulting in hybrid orbitals that share character of both 2s and 2p orbitals. Hybrid orbitals are represented as 2sp, $2sp^2$ or $2sp^3$, depending on how many p orbitals have taken part in hybridization. Carbon atom with four $2sp^3$ hybrid orbitals, forms a tetrahedral structure with bond angles close to 109.5 degrees like the one in methane, CH_4 (figure 6.2 A), carbon atom with three $2sp^2$ hybrid orbitals and one $2p_z$ orbital forms a planar structure with bond angles close to 120 degrees as is the case with ethene, C_2H_4 (figure 6.2 B), and carbon atom with two 2sp hybrid orbitals and one $2p_y$ orbital and one $2p_z$ orbital forms a linear structure with bond angles of 180 degrees as in ethyne, C_2H_2 (figure 6.2 C). The $2sp^3$, $2sp^2$ and 2sp hybrid orbitals point toward neighbouring atoms forming σ bond to them, whereas the 2p orbitals are perpendicular to these σ bonds and form π bonds to the neighbouring atoms. [32, pp. 29–105; 34, pp. 105–107]

In graphite, graphene and CNTs carbon atoms are $2sp^2$ hybridized. $2sp^2$ hybridization can be seen in figure 6.1. This $2sp^2$ hybridization explains the hexagonal structure of these allotropes.

6.1.2 Structure of CNTs

Carbon nanotubes are long, narrow tube-like structures that are composed only of carbon atoms. The ratio of length to diameter of CNTs is one of the largest of known molecules. CNTs can be either single-walled (SWNTs) or multi-walled nanotubes

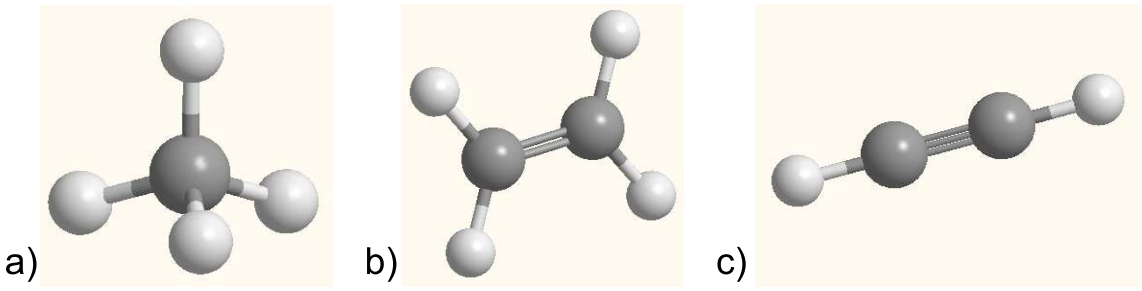

Figure 6.2. *a) $2sp^3$ hybridized structure of methane, b) $2sp^2$ hybridized structure of ethene and c) 2sp hybridized structure of ethyne.*

(MWNTs). Diameter of a SWNT is usually between 0.6 and 2.0 nm. Smaller nanotubes have large strain energy due to the curvature and bigger SWNTs tend to collapse. For MWNTs diameter of the innermost tube is usually larger than 2 nm and diameter of the outermost tube is usually less than 100 nm. This is possible, because in MWNT all nested tubes are surrounded by other tubes. The length of a CNT can be up to 10^5 times its diameter. [33, p. 35; 35, p. 5]

The structure of a SWNT can be thought as a graphene (single layer graphite) sheet rolled in cylindrical shape. SWNTs have three main structural forms: armchair, zig-zag and chiral (figure 6.3). Which structural is formed depends on what direction the graphene sheet is rolled.

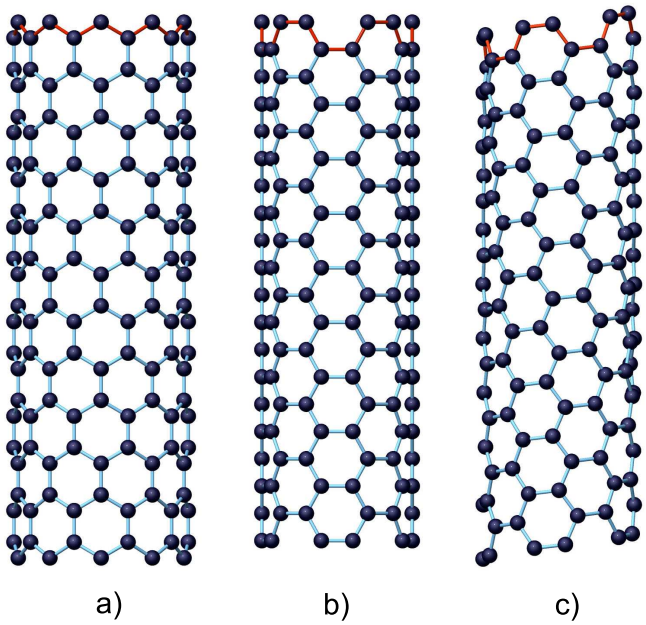

Figure 6.3. *Structures of a) zigzag, b) armchair and c) chiral SWNTs. [36]*

In figure 6.4 the formation of a SWNT is illustrated. Vectors $\mathbf{a}_1$ and $\mathbf{a}_2$ are the basis vectors with which the structure of the nanotube is expressed. If the graphene

sheet is rolled in the direction of $\mathbf{a}_1$ vector, a $(n, 0)$ or zigzag nanotube is formed. If instead graphene is rolled in $\mathbf{a}_1 + \mathbf{a}_2$ direction, a (n, n) or armchair nanotube is formed. Both, zigzag and armchair SWNTs are achiral since their mirror image has the same structure as the original one. Chiral nanotubes (n, m) are spiral and their mirror image differs from the original one. Chirality of a nanotube is described by chiral vector $\mathbf{C}_h$. For the nanotube that is formed in figure 6.4 the chiral vector would be $\mathbf{C}_h = 5\mathbf{a}_1 + 2\mathbf{a}_2$. [33, pp. 37–38]

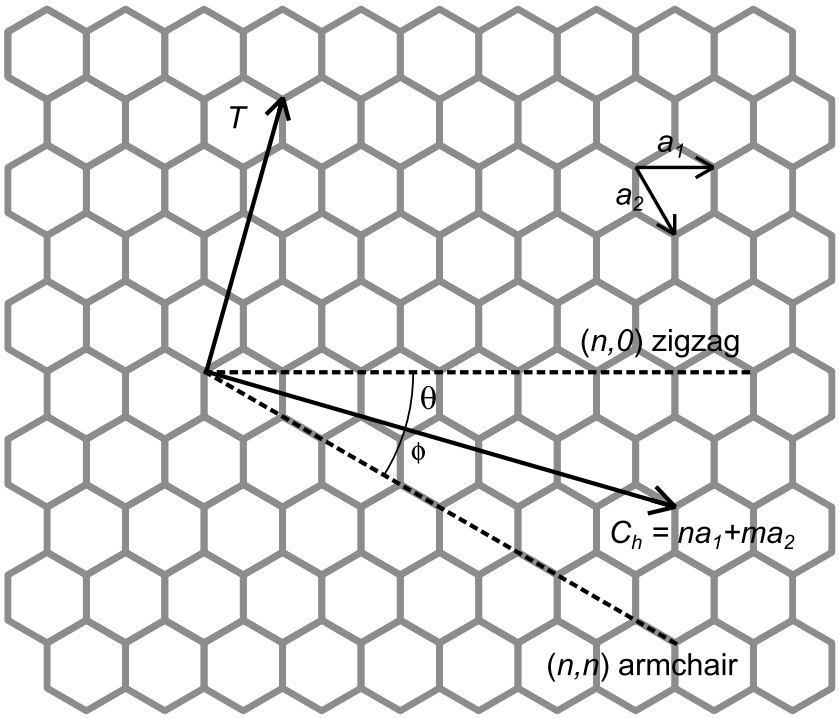

Figure 6.4. *Chiral vector of CNT.*

In graphene carbon atoms are located in the corners of the regular hexagons of which graphene consists of. Distance between two carbon atoms in graphene is $a_{C-C} = 0.1421$ nm. From the geometry of regular hexagon the length of the basis vectors $\mathbf{a}_1$ and $\mathbf{a}_2$ can be calculated to be $a = |\mathbf{a}_1| = |\mathbf{a}_2| = \sqrt{3}a_{C-C} = 0.246$ nm.

If we represent the unit vectors in unit vectors of x-y-plane ($\hat{\mathbf{i}}$ and $\hat{\mathbf{j}}$) we get

$$\mathbf{a}_1 = (\hat{\mathbf{i}}, 0)\, a \text{ and } \mathbf{a}_2 = \left(\frac{1}{2}\hat{\mathbf{i}}, -\frac{\sqrt{3}}{2}\hat{\mathbf{j}}\right) a \tag{6.1}$$

Now we can calculate the length, L_c, of the chiral vector of a (n, m) nanotube, which is also the circumference of the nanotube.

$$L_c = |\mathbf{C}_h| = |n\mathbf{a}_1 + m\mathbf{a}_2| = \left| n\,(\hat{\mathbf{i}}, 0)\, a + m\left(\frac{1}{2}\hat{\mathbf{i}}, -\frac{\sqrt{3}}{2}\hat{\mathbf{j}}\right) a \right| \tag{6.2}$$

If we further rearrange equation 6.2, we get

$$L_c = a \left| \left(n + \frac{1}{2}m \right) \hat{\mathbf{i}} + \left(-\frac{\sqrt{3}}{2}m \right) \hat{\mathbf{j}} \right| \tag{6.3}$$

$$L_c = a \sqrt{\left(n + \frac{1}{2}m \right)^2 + \left(-\frac{\sqrt{3}}{2}m \right)^2} \tag{6.4}$$

$$L_c = a\sqrt{n^2 + m^2 + nm}. \tag{6.5}$$

From equation 6.5 we can easily calculate the diameter of an individual SWNT that has a chiral vector of (n, m)

$$d_t = \frac{L_c}{\pi} = \frac{\sqrt{n^2 + m^2 + nm}}{\pi} a. \tag{6.6}$$

Vector $\mathbf{T}$ (figure 6.4) is the translational vector that is parallel to the nanotube axis and normal to the chiral vector $\mathbf{C}_h$. Translational vector $\mathbf{T}$ can also be expressed using the basis vectors $\mathbf{a}_1$ and $\mathbf{a}_2$ as follows

$$\mathbf{T} = t_1\mathbf{a}_1 + t_2\mathbf{a}_2 \equiv (t_1, t_2), \tag{6.7}$$

where t_1 and t_2 are integers that are expressed as follows

$$t_1 = \frac{2m + n}{d_R} \text{ and } t_2 = -\frac{2n + m}{d_R}, \tag{6.8}$$

where d_R is the greatest common divisor of $(2m + n)$ and $(2n + m)$. By using equations 6.7 and 6.8 the translational vector corresponding to chiral vector (5,2) (figure 6.4) to be $\mathbf{T}$ = (3,-4). The length of vector $\mathbf{T}$ is

$$T = |\mathbf{T}| = \sqrt{3}/d_R. \tag{6.9}$$

Vectors $\mathbf{C}_h$ and $\mathbf{T}$ define the rectangular unit cell of the nanotube. The area of the cell is the absolute value of the cross product of these two vectors, $|\mathbf{C}_h \times \mathbf{T}|$. The area of a single hexagon is $|\mathbf{a}_1 \times \mathbf{a}_2|$. The number of hexagons in a unit cell, N, can be calculated by following equation

$$N = \frac{|\mathbf{C}_h \times \mathbf{T}|}{|\mathbf{a}_1 \times \mathbf{a}_2|} = \frac{2(m^2 + n^2 + nm)}{d_R} = \frac{2L_c^2}{a^2 d_R}, \tag{6.10}$$

where L_c is given in equation 6.5, a is the length of the unit vectors and d_r is the greatest common divisor of $(2m + n)$ and $(2n + m)$. Because there are two carbon atoms in each hexagon, the total number of carbon atoms in a unit cell of SWNT is $2N$. [33, pp. 37–46]

MWNTs consist of two or more nested SWNTs. Spacing between adjacent layers of MWNT is very often roughly the interlayer spacing in graphite which is 0.335 nm [37, p. 45]. In most cases the structures of concentric SWNTs that form a MWNT are not commensurate to each other. Actually the only commensurate cases are the one that are build of only armchair or of only zigzag SWNTs since then they will have the same translational vector $\mathbf{T}$. [33, p. 222]

6.1.3 Properties of CNTs

CNTs have many extraordinary properties. Their tensile strength can be up 150 GPa, which is almost 400 times that of steel [35, p. 15]. In addition CNTs are three to six times less dense than steel [35, p. 15]. Flexibility and electrical properties of CNTs are of the main interest in this work, because they are used as electrode materials in flexible pressure sensors.

Electrical properties of CNTs depend greatly on the chirality and diameter of the tubes [33]. As was mentioned in section 6.1.1 each carbon atoms in graphene have three sp^2 hybridized orbitals and one p orbital. Electrons on the sp^2 orbitals form σ bonds with the three neighbouring carbon atoms thus forming a strong hexagonal honeycomb structure that is characteristic for graphene. The p orbital is perpendicular to the graphene sheet. The π electrons on the p orbitals are delocalized i.e. they can move along the graphene plane which makes graphene electrically and thermally conducting. [35, pp. 2–3]

When a SWNT is formed by rolling up a graphene sheet the bonding remains essentially sp^2 hybridized. However, this causes the σ bonds to get slightly out of plane. This change is compensated by delocalizing the π orbital more outside the tube. The change in π orbital's structure is responsible for increment of electrical and thermal conductivity and mechanical strength compared to that of graphite. [35, pp. 2–3]

The theory behind the electric structure of SWNTs is long and complicated and will therefore not be discussed in details in this thesis. For further interest read reference [33]. For simplification can be said that about one third of SWNTs are metallic (no band gap) and two thirds of SWNTs are semiconducting (a small band gap). Categorization of SWNTs into these two categories can be made by looking the integers (n, m) of the chirality vector $\mathbf{C}_h$. If $n - m$ is a multiple of 3, the nanotube is metallic. This is the case for all armchair nanotubes ($n = m$) and for one third of the zigzag and chiral nanotubes, although it is found that $\sigma - \pi$ rehybridization can open a small band gap ($\sim$0.02 eV) in small-diameter ($<$1.5 nm) nonarmchair metallic SWNTs.

The rest of the SWNTs are semiconductors i.e. in the case where $n - m = 3q \pm 1$, where q is an integer. For semiconducting SWNTs the band gap, E_g, can be

calculated by using following equation

$$E_g = 2a_{C-C}\gamma/d_t, \tag{6.11}$$

where γ is the nearest neighbour-hopping parameter which has values from 2.5 to 3.2 eV in literature. [33, pp. 68–69; 35, pp. 9–10]

The results of electrical properties derived for a SWNT cannot be applied to MWNTs directly. Intertube coupling between the nested tubes needs to be taken in consideration, especially in small diameter MWNTs. This intertube coupling can, for example, open a small band gap in two nested metallic nanotubes making them both semiconducting. When the diameter of the tubes increases, the intertube coupling decreases. In general for MWNTs the largest, outermost tube dominates the electrical properties and therefore characterizes the MWNT to be either metallic or semiconducting. [35]

6.1.4 CNT solutions

In order to print CNTs on a substrate CNTs have to be dispersed into a solvent such as water or organic solvent. Making a dispersion of CNTs is not as simple as one might think. Due to the long tubular structure CNTs are able to settle next to each other, which induces strong attractive van der Waals interactions between the tubes. These interactions cause the CNTs to form aggregates. [38, 39]

Ultrasonication is commonly used to overcome the van der Waals interactions thus dispersing the CNTs throughout solvent. The obtained dispersion is not stable in any solvent, though, and the CNTs start to reagglomerate in solvent. Stability of the dispersion in water can be improved in several ways. One way is to use surfactants such as SDS. In aqueous SDS/CNT solutions SDS molecules surround individual CNTs. The hydrophobic tails of the SDS molecules point toward the CNTs and the hydrophilic heads that stick out toward the water phase keep the CNT water disperseable preventing the CNTs from agglomerating. [38, 39]

Another way to improve the dispersebility of CNTs in water is to use nanocellulose or cellulose derivatives. Cellulose is the most abundant polymer in the world [40]. It is found in high proportion in renewable sources such as plants. Also bacteria can be used to produce cellulose [41]. In order to improve the dispersebility of CNTs cellulose has to form a nanocomposite with CNTs. In nanocomposite two different solid materials interact at molecular level. In order for this to happen the size of cellulose has to be comparable to that of CNTs. [40, 42]

The size of cellulose fibers found in wood pulp (width 30 to 40 μm, length 1 to 3 mm) [43] is much larger than that of CNTs (section 6.1.2). However, the size of nanofibrillated cellulose or nanocellulose (width 5 to 30 nm, length over 1 μm) [43] is

comparable to that of CNTs and is therefore suitable for dispersing them. Cellulose produced by bacteria is directly in form of nanocellulose [41]. The macroscopic cellulose fibres in wood pulp can be broken up into nanocellulose mechanically, for example. One way to make a CNT nanocellulose nanocomposite is the following. First, CNTs and cellulose pulp is ground together in a mortar to brake bigger CNT agglomerates. Second, ultrasonication is used to break up the CNT bundles and cellulose molecules (nanocellulose) from the fibers. Finally, nanocomposite is formed when nanocellulose winds around CNT. [40]

As was said earlier also cellulose derivatives can be used to disperse CNTs. What distinguishes cellulose derivatives from pure cellulose is that some of the hydrogen atoms of the hydroxyl groups of a cellulose molecule are replaced with another substituent. The cellulose derivative that was used in some of the inks in this work is carboxymethyl cellulose (CMC). In CMC some of the hydrogen atoms of the hydroxyl groups are replaced with carboxymethyl substituent (-CH_2COOH). The repeating units of cellulose and CMC can be seen in figure 6.5. [42]

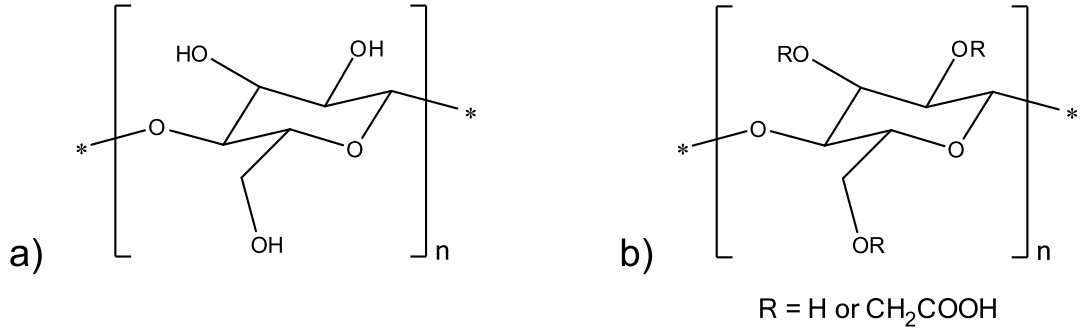

Figure 6.5. *Structure of repeating unit of a) cellulose and b) carboxymethyl cellulose.*

In both nanocellulose and CMC the capability to disperse CNTs is based in their tendency to wind around CNTs. The polar groups in nanocellulose and CMC make CNTs more disperseable into polar solvent, such as water and also prevent the individual CNTs to agglomerate together.

6.2 Silver inks

Silver has the smallest electrical resistivity ($\rho = 1.467 \cdot 10^{-8}$ Ωm at $T = 273$ K) of all known metals [44] and is therefore often used as a conductor in electronics. In silver inks that are used in printed electronics, silver is dispersed as small particles throughout the ink. The average particle size can vary from tens of nanometers to micrometers.

During printing silver ink is deposited on a substrate. At this moment silver appears in particles rather than in a uniform bulk layer. This leads to conductivity

that is significantly less than that of bulk silver. In order to increase the conductivity the ink has to be sintered during which small particles weld together below the melting point of bulk silver. Sintering rate depends on the size of the particles, being greater for smaller particles. Even though sintering temperature can be decreased by using smaller particles, it is too high (150°C) for even silver nanoparticle inks to be used with piezoelectric PVDF. At elevated temperatures piezoelectric PVDF substrate shrinks and experiences a loss in its piezoelectricity. [2]

6.3 PEDOT:PSS inks

When one sees the word polymer one will most likely think about the polymers used in everyday plastics, such as polyethylene (PE) or polyvinylchloride (PVC). Those polymers are good insulators and it could form an illusion that all polymers are insulators. Actually, that was pretty much the case before 1970s and polyacetylene. In the end of the decade scientist discovered that doped form of polyacetylene can have conductivity of up to 100 S/m. This discovery has led to massive research on the field of conducting polymers which has resulted in discovery of various conducting polymers (CP), such as the one used in this work: poly(3,4-ethylenedioxythiophene) (PEDOT). And now, when talking about CPs only the polymers that are intrinsically conductive are taken in to account, not the conductive blends of polymers and metal or carbon powders. [45]pp. 4–9galvin1997electrically

6.3.1 Conductive polymers

Conductivity of PEDOT, and of other CPs, arises from the structure of their carbon backbone in which double and single bonds alternate. Polymers with such structure are called conjugated polymers and their electrons can be delocalized over many carbon atoms on the chain, just like they are delocalized in a benzene ring. However, conjugated structure of a polymer alone does not make the polymer conducting. Without doping these polymers would be insulators.

With CPs when talking about improving conductivity of the polymer by doping, a different procedure is meant than the one used when doping inorganic semiconductors resulting in increment in their conductivity. Inorganic semiconductors are doped by adding small amounts (parts per million) of donor (pentavalent) or acceptor (trivalent) impurities, which will provide negative (electrons) or positive (holes) charge carriers in the semiconductor, respectively. This will have an enormous effect on semiconductors conductivity.

When doping conjugated polymers large amount of electrons are added or removed from the conjugated chain. First the conductivity increases dramatically with increasing doping but eventually it will saturate at certain level. Doping of a

conjugated polymer can be made in several ways.

Chemical doping is one way to make CPs. In chemical doping a chemical, to which the polymer is exposed, reduces (adds electrons) or oxidizes (removes electrons) the polymer resulting a net charge in the polymer. Halogens, for example, are used to oxidize polymers. A major disadvantage in chemical doping is its poor controllability. In electrochemical doping reduction and oxidation reactions are controlled by altering the voltage between the CP and the counter electrode. [46]

6.3.2 PEDOT:PSS

PEDOT was the conducting polymer that was used in work. Pure PEDOT has very low solubility to water and therefore polystyrene sulfonate (PSS) is used to form water-soluble PEDOT:PSS. Structure of PEDOT:PSS can be seen in figure 6.6. Doping has removed electrons from PEDOT and therefore it has a positive charge. Negative charge on PSS results from deprotonation of some of the sulfonyl groups in it.

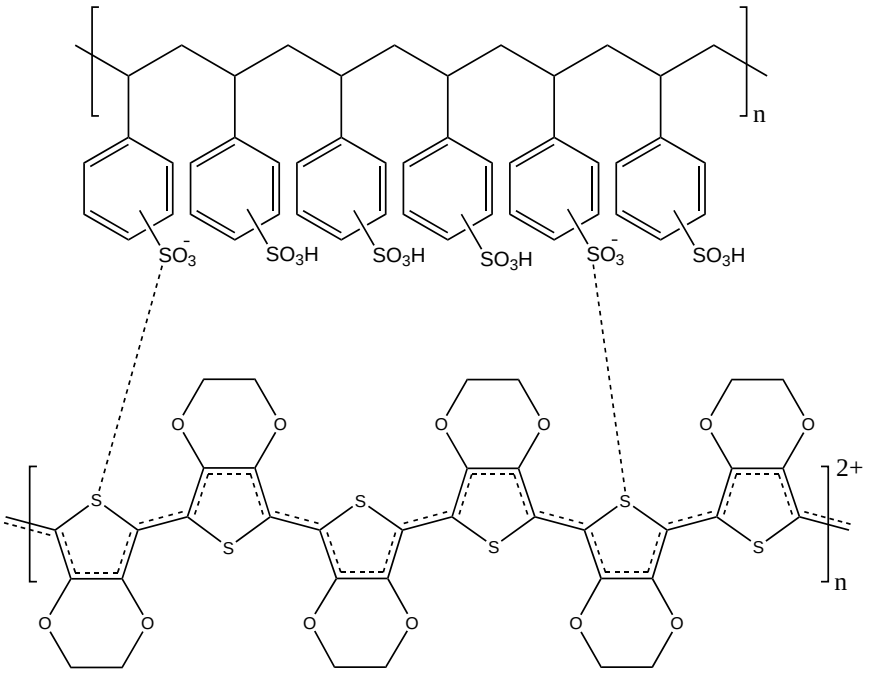

Figure 6.6. *Structures of PEDOT (lower polymer chain) and PSS (upper polymer chain), which together form PEDOT:PSS.*

Although PEDOT is considered as a CP, pristine PEDOT:PSS yields quite low conductivities, in the range of 0.1 to 10 S/cm. There are some simple and effective methods that can improve the conductivity of a deposited PEDOT:PSS film remarkably.

Addition of dimethyl sulfoxide (DMSO), ethylene glycol (EG) or some other high-boiling-point polar solvent into a PEDOT:PSS solution can improve the conductivity of PEDOT:PSS up to three orders of magnitude. The mechanism that leads to this change in conductivity is not known for sure. According to one theory some of the solvent remains in PEDOT:PSS inducing a screening effect that will reduce the Coulomb interaction between positive PEDOT and negative PSS chains [47]. [48]

Anionic surfactants can also be used to improve the conductivity of PEDOT:PSS. According to Fan et al. by adding SDS to a PEDOT:PSS solution the conductivity may increase up to 500 times compared to that of pristine PEDOT:PSS. In their theory SDS molecules replace the PSS molecules as counter anion for PEDOT. Normally, in aqueous solution PEDOT chains have to follow the structure of PSS chains. Because the repeating unit of PEDOT is longer than that of PSS this will distort the PEDOT chains thus decreasing conductivity. When SDS molecules replace PSS chains, distortion of PEDOT chains disappears resulting in improvement of conductivity. [49]

Improvements on the conductivity of a PEDOT:PSS film can be also done after the deposition of the film. Kim et al. have received conductivities as high as 1418 S/cm for a PEDOT:PSS film, by using a method called solvent post-treatment. In the treatment PEDOT:PSS films were immersed into an EG bath for different periods of time. The solvent post-treatment not only had improving effect on the conductivity but also in the stability against air-exposure. The magnitudes of those effects were time-dependent, being the bigger the longer the films were immersed in the EG bath. According to the research and experiments carried out by Kim et al. the improvement of conductivity results from the removal of insulating PSS. They based their results on transmittance measurements, atomic force microscope (AFM) pictures and X-ray photoelectron spectra. [48]

7. MATERIALS AND FABRICATION

Most of the inks used in this work can be divided in three classes: CNT inks, silver inks and PEDOT:PSS inks. More specified formulations of all the inks used in this work can be found in appendix A. In order to get a working piezoelectric pressure sensor, the ink must be printed on piezoelectric PVDF. In this work samples were also printed on non-piezoelectric polyethylene terephthalate (PET) and polycarbonate (PC) substrates just to test the ink properties. Printability on those substrates differs from that of on PVDF, but because PET and PC are much more inexpensive materials and easier available, this was a reasonable procedure.

7.1 Inks

In this thesis most of the inks were not actually inks, rather solutions that contained conducting component. Commercial inks have various additives and are designed for printing and therefore their printability is good. Commercial inks for the research done in this work were not available and therefore plain solutions had to be used. Some additives were used in formulations to improve the printability of the solutions.

7.1.1 CNT inks

All CNT inks used in this thesis were based on CNT solutions that were received from our collaborator Pasi Moilanen [50]. CNT solutions were printed as received or after some modifications that were made to improve printability. Most common solvent in the CNT solutions that were used was water. Advantages for using water as a solvent are that it is cheap and non-toxic. Disadvantages, on the other hand, are fairly slow evaporation rate, which leads to slow drying of water-based inks and poor wettability of most substrates due to high surface tension.

Plain CNTs have very poor dispersability in water. That is why instead of having plain CNTs, a nanocomposite of CNTs and CMC was used. A nanocomposite is not just a rough mixture of CMC and CNT. Instead CMC molecules interact with CNTs at molecular level wrapping around them. This is possible due to the similar size of CMC and CNT molecules.

In preliminary mixing bigger agglomerates of CMC and CNTs can be broken in a mortar. Next solvent is added and sonication is used to break up bundles so that nanocomposite can be formed. Polar groups of CMC molecules improve the stability

of the nanocomposite dispersion compared to that of plain CNTs.

There were a few CNT solutions that were used as a base for the CNT inks that were formulated in this thesis. These CNT solutions and their composition can be found in table A.1 in appendix A. Nano-4 and Nano-5 solutions are made by evaporating water from Nano-1 solution. New solids content percentages are calculated for them. Composition of CNT inks formulated from CNT solutions can be found in table A.2 in Appendix A.

7.1.2 Silver inks

All silver ink formulations in this thesis were based on Henkel's Electrodag PM-460A silver ink. Solids content of this ink is 72 % containing n-Propylacetate as solvent. The viscosity of plain Electrodag PM-460A is too high (4000 cP at 20 °C) for flexographic printing and must therefore be reduced by solvent addition. Propylene glycol monomethyl ether acetate (PGMEA) was used as additive solvent. Different silver ink formulations that were prepared for this thesis can be found in table A.3 in Appendix A.

In silver ink preparation constituents were measured and put in a small glass jar. Because silver particles are heavy and tend to sediment at the bottom of the jar, thorough mixing is necessary in silver ink preparation before ink is ready to be printed. Mixing was carried out on magnetic stirrer for several hours or overnight.

7.1.3 PEDOT:PSS inks

PEDOT:PSS inks that were used in this thesis were prepared by modifying two commercial liquid PEDOT:PSS products. Both of these were products of H.C. Starck GmbH. Clevios™ FE is blue aqueous dispersion of PEDOT:PSS containing organic solvents and polymeric binders, having solid content of 3.0 to 4.0 % [51]. Baytron™ PH 500 is blue aqueous dispersion of PEDOT:PSS having solid content of 1.0 to 1.3 % and PEDOT:PSS ratio of 1:2.5 by weight [52].

Because both Clevios™ FE and Clevios™ PH 500 are water-based (high value of surface tension, $\gamma_{\text{water}} = 73.05$ mN/m at 18 °C [44]), their wettability and printability have to be improved in order for using them as printing inks on hydrophobic polymer substrates such as PVDF. SDS and isopropanol (IPA) ($\gamma_{\text{IPA}} = 21.7$ mN/m at 20 °C [44]) can be used to lower surface tension. Other additives that were used were DMSO, EG and polymer solution P-1. For further information about P-1, see reference [53]. Although the surface tensions of DMSO and EG are lower than that of water, the main reason for adding these two substances is their enhancing effect on conductivity of printed PEDOT:PSS film. Ink formulations based on Clevios™ FE can be found in table A.4 in Appendix A. Ink formulations based on Baytron™

PH 500 can be found in table A.5 in Appendix A.

7.1.4 PEDOT:PSS/CNT inks

Promising results in a former study by Yun et al. [54] encouraged making tests with CNT/PEDOT:PSS composite ink. The composite inks were simply formulated by mixing Nano-1 CNT-solution and Clevios™ FE PEDOT:PSS-solution. In some inks also SDS was added. More specific information about the ink composition can be found in table A.6 in Appendix A.

7.2 Substrates

Three different polymer substrates (PET, PC and PVDF) were used in this thesis. Although only PVDF can be used when fabricating pressure sensors, printing on PET and PC (which are much cheaper substrates) gave plenty of useful information of the inks' properties such as printability and conductivity. PVDF has lower surface energy ($\gamma_{\mathrm{PVDF}} = 30.3$ mN/m [55]) than PET ($\gamma_{\mathrm{PET}} = 44.6$ mN/m [55]) and PC ($\gamma_{\mathrm{PC}} = 34.2$ mN/m [55]) have and is therefore more hydrophobic and more challenging to print on. Contact angles between water and PET (68.2 ± 0.4 degrees) and water and PVDF (75.0 ± 1.6 degrees) were measured also in this work using Krüss DSA30 Contact Angle Measuring Instrument. These results also state that PVDF is more challenging to print on. UV ozone treatment can be used to increase the surface energy of all these substrates making them more hydrophilic and thus making them easier for inks to wet.

PET substrate that was used in this thesis was 125 µm thick Melinex® ST506 of DuPont Teijin Films. PET substrate is transparent and fairly easy to handle because of its moderate thickness.

PC substrate was 175 µm thick. PC substrate is transparent and because it is fairly thick it is also easy to handle. More detailed information about this substrate is not available.

PVDF substrate that was used in this thesis was Measurement Specialties 28 µm thick PVDF Piezo Film. PVDF substrate is transparent and due to its thinness quite hard to handle because it tends to wrinkle quite easily. Detailed information about the PVDF substrate can be found in table 5.1.

7.3 Sample fabrication

Clean surface of a substrate is necessary for good printing quality and ink adhesion. In most cases substrates were cleaned by rinsing them with IPA and let dry thoroughly. Next, for most samples, UV ozone treatment was used to increase surface energy of the substrate. Ink was deposited on the substrate by RK flexiproof 100

or CX202 motorized bar coater. In following subsections sample preparation and possible problems that occurred during sample fabrication are shortly discussed. Sample name tells some details about the sample. First letter(s) presents the ink type (N = (carbon)nanotube, S = silver, P = PEDOT:PSS, C = carbon, PN = PEDOT:PSS/CNT) and the second letter presents the fabrication method (F = flexo, B = bar coating). The number at the end distinguishes samples from each other.

7.3.1 Samples printed with RK Flexiproof 100

Printing samples with RK Flexiproof 100 appeared challenging. Inks tended to dry on the anilox, clogging the tiny cells on the surface of the anilox. This reduced the amount of ink transferred to the substrate thus making the printed conducting layer thinner. Thinner conducting layer means higher sheet resistance.

The effect of the ink clogging can be avoided or at least reduced by cleaning the anilox properly between each print. Thorough cleaning often required removal of the anilox and plate rolls. Another problem was observed when the rolls were removed and put back in place. There seemed to be some clearance between the roll and the axis that hold them in place. The rolls were almost impossible to attach at their former places, which caused changes in printing and ink transfer. Pressure between the rolls changed although readings on the adjustment screws were left untouched. Uneven pressure distribution or too high impression pressure during the printing process resulted in uneven ink distribution on the substrate. In many samples this can be seen as thicker ink line at the rear section of the printed electrode.

CNT samples

CNT inks were really challenging to print with RK Flexiproof 100. Hydrophobicity of the substrates, especially PVDF, made substrate wetting hard for water-based CNT inks. Surface treatment of the substrate with UV ozone and surfactant additions to the inks improved wetting though. Also increment in the ink viscosity seemed to lead to better printing quality. Information about the flexo printed CNT samples can be found in table B.3 in appendix B. Printing speed for all CNT samples was 20 m/min. Anilox pressure of 125 was used. Impression pressure was 95 for PVDF samples.

When CNT inks were flexo printed on substrates they seemed to form stripes or patterns of width about 0.5 mm, in which darker and lighter areas alternate. These stripes are aligned in the printing direction. Even though it seemed that the ink was distributed unevenly on the substrate, the electric properties of the printed electrodes seemed quite even i.e. the standard deviations (STDEV) of the sheet resistance values of most electrodes were fairly small as can be seen in section 8.1.1.

Uneven flexo printing quality of CNT samples can be seen in figure 7.1.

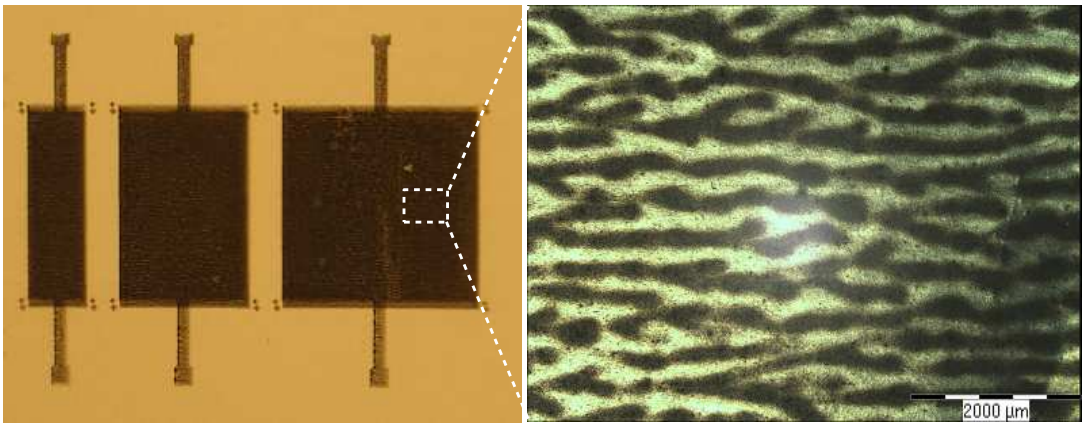

Figure 7.1. *On the left is picture of flexo printed CNT sample N-F-1. On the right microscope picture of the same sample where the stripes or patterns that are formed during printing are clearly visible. The sample in the picture is printed with old flexographic plates and has therefore I-shaped extensions instead of the L-shaped extensions that appear in newer plates.*

Silver and carbon samples

Flexographic printing of silver flake inks appeared really challenging. Silver inks clogged the anilox cells really fast and therefore ink transfer to the substrate was quite poor. No good results were obtained for flexo printed silver electrodes in either sheet resistance or sensitivity measurements. Yellow Miraclon BF plate was used for printing. Solvent for all samples was PGMEA.

One PVDF sample (C-F-1) was printed with carbon ink (purchased from Creative Materials). The ink is a resistive ink and made for flexographic printing. The quality of the ink was not really good, because it was quite old when printed. Carbon sample was also printed for several times, which increases the layer thickness and therefore decreases the sheet resistance.

PEDOT:PSS samples

Substrate hydrophobicity was a problem with water-based PEDOT:PSS inks just as it was with the CNT inks. SDS was used in many inks to overcome this problem. Transparency of the PEDOT:PSS layers made observing the printing quality with the naked eye quite tricky. Therefore adjusting the printing parameter was difficult. All flexo printed PEDOT:PSS samples were printed using green ASAHI flexographic plate and 20.1 cm^3/m^2 chrome anilox. For printing PEDOT:PSS samples anilox pressure from 120 to 125 was used. Impression pressure depended greatly on the

substrate thickness. For 125 µm PET substrate impression pressures from 110 to 115 were used. For 175 µm PC substrate impression pressure from 115 to 125 was used. For 28 µm PVDF substrates impression pressure was 90. Printing speed was 20 m/min.

Before printing, all substrates were washed with IPA and treated with UV ozone for 5 minutes. PVDF substrates were treated 5 minutes on both sides. Some PEDOT:PSS samples were immersed in ethylene glycol bath after printing to improve their conductivity. Detailed information about flexo printed PEDOT:PSS samples can be found in table B.2 in appendix B.

When printed with flexo, similar stripes that occurred in flexo printed CNT samples occurred also in PEDOT:PSS samples. No pictures of flexo printed PEDOT:PSS samples are represented here because PEDOT:PSS is nearly invisible.

7.3.2 Samples prepared with CX202 motorized bar coater

Sample preparation with CX202 appeared much easier than with RK Flexiproof 100. Moderate film quality was also achieved in many samples. Although CX202 is a handy apparatus, one must remember that some results obtained with it are non-reproducible with flexographic press. All samples were prepared with speed 50 mm/s.

CNT samples

6 µm bar was used when CNT samples were prepared. CNT inks offered challenge also when using CX202. Immediately after application most films appeared quite even but in some samples the wet film of ink started to withdraw. This was most likely due to too high surface tension of the ink (or too low surface energy of the substrate). This problem was tried to solve by adding SDS to the ink. Visual quality of the films was slightly improved with water based inks, but when SDS was added to inks that contained ethanol, film quality dropped even more. Information of CNT samples prepared with CX202 can be found in table C.1 in appendix C.

Silver samples

Depositing silver ink with CX202 appeared much easier than flexographic printing. Film applied CX202 was visually quite uniform and had low sheet resistance, as can be seen in section 8.1.

PEDOT:PSS samples

All bars (4 µm, 6 µm, 10 µm and 12 µm) were used in preparing PEDOT:PSS samples. For preparing PEDOT:PSS samples, CX202 worked tolerably. Visual

evaluation of PEDOT:PSS samples is quite challenging, though. This is because prepared PEDOT:PSS films are transparent.

In some samples ink formed stripes, similar to those that appeared in flexo printed samples. On the other hand some samples showed really uniform quality.

PEDOT:PSS/CNT samples

All PEDOT:PSS/CNT samples prepared with CX202 have fairly good and uniform quality. Samples PN-B-5 to PN-B-8 have higher CNT concentration than samples PN-B-1 to PN-B-4 and therefore some darker stripes occur in those samples. No major visible difference can be seen between samples that are prepared with inks containing SDS and the ones prepared with inks that do not contain it. Because all samples were prepared on PET substrate, suitability on PVDF has to be studied in further studies.

8. MEASUREMENT AND ANALYSIS

Various measurements, tests and analysis were carried out to get information about used inks and the sensor elements printed with the inks. Although plenty of data was collected from different measurement, information about film layer thickness and uniformity appeared very hard to get. This information would have enabled better comparison of electrical properties of different films.

8.1 Results of sheet resistance measurements

Sheet resistance of a printed sample was measured using four-point probe and Keithley 2425 (chapter 4). Corrections on the value of R_S were made depending of the size of the sample (table 4.1). Each sample was measured at five spots. Sheet resistance was measured at each of these spots both vertically and horizontally, so total of ten measurements were made on each side of a sample (samples on PET and PC have ink only on one side, PVDF samples have ink on both sides). Average values and STDEVs of R_S were calculated from these measurements.

8.1.1 CNT electrodes

The R_S values of CNT samples prepared with CX202 motorized bar coater are mainly in the range from 5 to 15 $k\Omega/\square$ as can be seen in figure 8.1. The film quality is visibly poor in samples N-B-9 and N-B-10. Ink that was used to fabricate these two samples was the only ink that contained both ethanol and SDS, so their incompatibility may have been the reason for the poor sample quality.

One thing that seems to effect the R_S value of the samples is the substrate material. In figure 8.1 of the samples N-B-1 to N-B-10 the even numbered ones are fabricated on PC and odd numbered ones on PET. All samples on PET have smaller value of R_S than the samples made with same ink on PC.

As was mentioned earlier in section 7.3.1, it was really challenging to print CNT samples with RK Flexiproof 100. Printing quality was often poor and uneven. The remarkable difference on sheet resistance between different electrodes of the same sample is one proof of this unevenness (figure 8.2). The printing quality of sample N-F-3 is visibly much poorer than that of samples N-F-1 and N-F-2, and is most likely the reason why its sheet resistance is also higher.

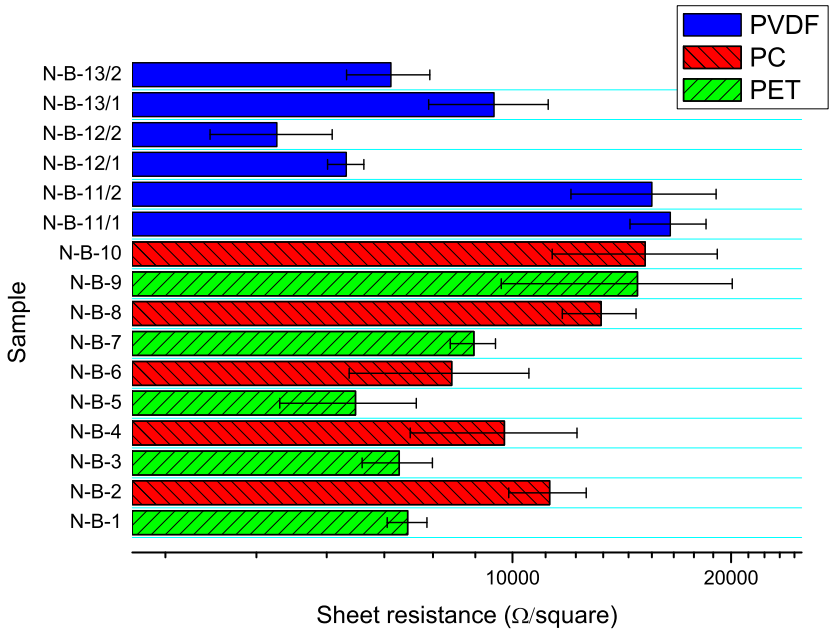

Figure 8.1. *Sheet resistance values of CNT samples applied with CX202 motorized bar coater. The error bars express the STDEV of sheet resistance values.*

8.1.2 PEDOT:PSS electrodes

The range of R_S for PEDOT:PSS samples is really wide. For bar coated samples based on Clevios™ FE values of R_S go from about 660 $\Omega/\square$ to about 640 $k\Omega/\square$ (figure 8.3). For bar coated samples based on Baytron™ PH 500 values of R_S go from about 790 $\Omega/\square$ to about 470 $k\Omega/\square$ (figure 8.4). For flexo printed samples based on Clevios™ FE values of R_S go from about 1100 $\Omega/\square$ to about 880 $k\Omega/\square$ (figure 8.5). The value of R_S depends, as observed below, mainly on the original PEDOT:PSS product that has been used, house-made ink formulation used, thickness of the deposited ink film and post-treatment of the printed sample. As observed in the literature, different commercial ink products yield different conductivities [56].

If a closer look is taken at samples P-B-1 to P-B-6 (same ink used in all six samples) in figure 8.3 one can see that the value of R_S increases when the film thickness decreases as expected. Some conclusions can also be made about the effect of UV ozone treatment on the R_S value. Of the six samples, the ones with odd number are UV ozone treated whereas the ones with even number are not. UV ozone treated samples have lower R_S value, except for P-B-5, but for it and for P-B-6 the values of STDEVs are so large that no reliable comparison can be made between the R_S values of these two samples.

Another, much more noticeable, effect on R_S is caused by EG post-treatment

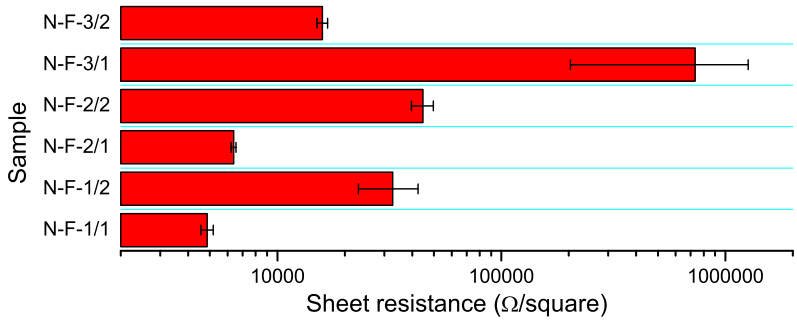

Figure 8.2. *Sheet resistance values of flexo printed CNT samples. The error bars express the STDEV of sheet resistance values.*

of the samples. The R_S values of P-B-17 and P-B-18 samples (with EG post-treatment) are over two orders of magnitude smaller than the R_S values of P-B-15 and P-B-16 samples (without EG post-treatment). The tremendous improvements in conductivities are compatible with the results that Kim et al. had on their study [48].

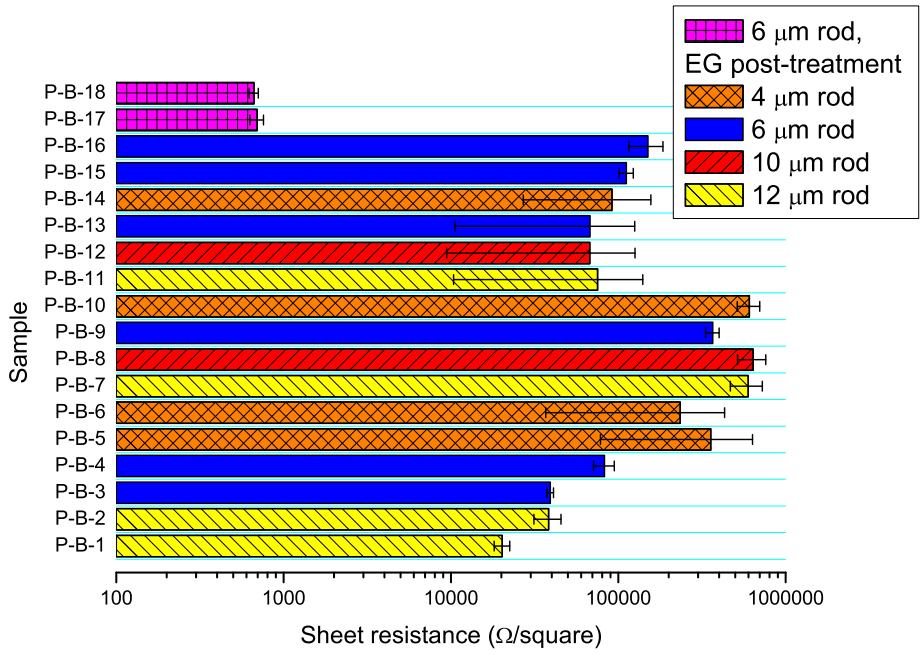

Figure 8.3. *Sheet resistance values of PEDOT:PSS samples based on Clevios™ FE. All samples are applied on PET substrate with CX202 motorized bar coater. The error bars express the STDEV of sheet resistance values.*

In figure 8.4 the effect of SDS and different solvents on the R_S value of PEDOT:PSS sample can be seen. Sample P-B-19 is made of pure Baytron™ PH 500.

Samples P-B-23 and P-B-27 have SDS added to them and it results in major improvement in conductivity. The R_S value for P-B-19 is 473 $k\Omega/\square$ whereas for P-B-23 and P-B-27 it is 24.7 and 6.92 $k\Omega/\square$ respectively.

The effect of solvent addition to Baytron™ PH 500 is also remarkable. Samples with EG (P-B-20, P-B-24 and P-B-28), DMSO (P-B-21, P-B-25 and P-B-29) or both EG and DMSO (P-B-22, P-B-26 and P-B-30) added to them show substantially (up to 595 times) smaller R_S values than the samples without added solvents (P-B-19, P-B-23 and P-B-27). In figure 8.4 it is not clear which solvent has the biggest effect on R_S but it seems that DMSO works slightly better than EG and adding both EG and DMSO works even better. One has to notice though than when both solvents are added the total volume of solvents added is double of that when only one solvent is added. So the results may not be perfectly comparable. From the results expressed in figure 8.4 one can clearly see that they are compatible with the results received from earlier studies [47–49].

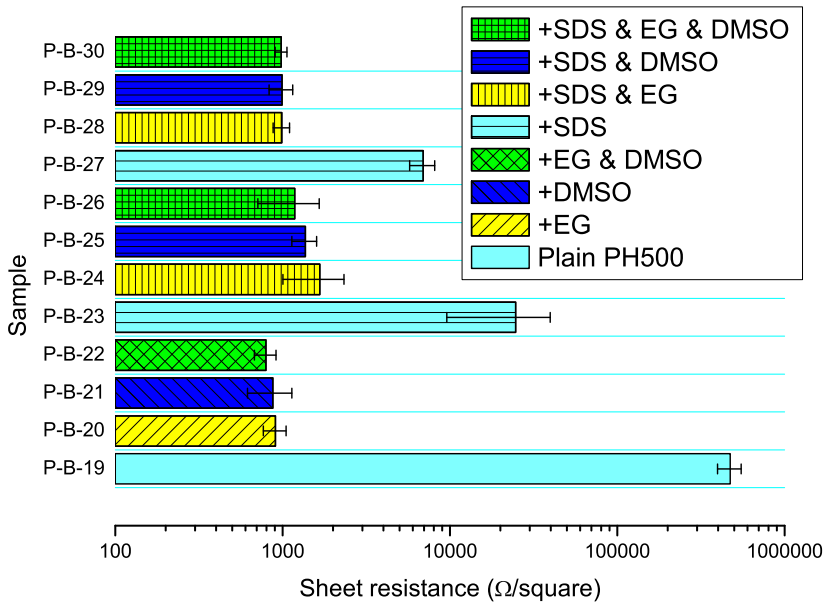

Figure 8.4. *Sheet resistance values of PEDOT:PSS samples based on Baytron™ PH 500. Samples are applied with CX202 motorized bar coater on PET substrate. The error bars express the STDEV of sheet resistance values.*

All flexo printed PEDOT:PSS samples were based on Clevios™ FE. Samples were printed on PET, PC or PVDF. Because the printing quality of RK Flexiproof 100 is not very even, the values of R_S in figure 8.5 should be treated with certain caution. From the R_S values of samples P-F-1 to P-F-6 the effect of EG post-treatment can be seen. The samples without EG post-treatment (P-F-1, P-F-4, P-F-10 and P-F-

11) have remarkably higher R_S than the samples with EG post-treatment (P-F-2, P-F-3, P-F-5, P-F-6, P-F-8 and P-F-9). This is compatible with results of Kim et al. [48].

Another, quite surprising, result that can be seen in figure 8.5 is that, in most cases, samples printed on PC have lower values of R_S than the samples printed on PET. What leads to this result is not known, because further research about the film thickness etc. was not made in this thesis. The unevenness of the printing quality can be seen when a closer look is taken at the R_S values of the PVDF samples (P-F-12 to P-F-14). The R_S of an electrode on one side of the substrate can be up to eight times bigger than the R_S value of the other electrode.

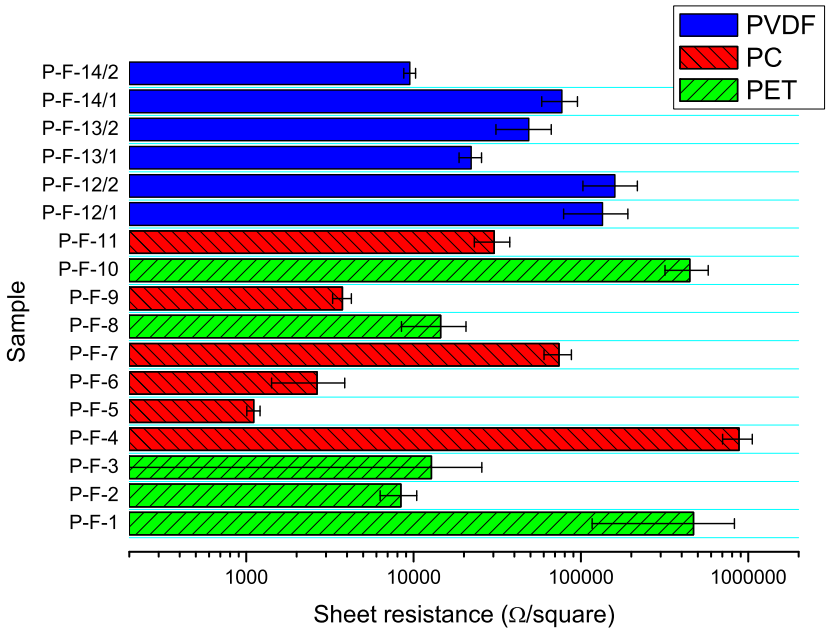

Figure 8.5. *Sheet resistance values of flexo-printed PEDOT:PSS samples. The error bars express the STDEV of sheet resistance values.*

8.1.3 Other electrode materials

Interesting but also rather predictable results were achieved with PEDOT:PSS/CNT samples on PET substrate. Sheet resistance values of those samples can be found in figure 8.6. The effect of EG post-treatment on sheet resistance is clear. Sheet resistance of the sample may drop up to 75 %.

Sheet resistance of EG post-treated sample PN-B-2 is lower than sheet resistance of any of those samples made with CNT or PEDOT:PSS only. Because the thickness of the conducting layer was not studied in this thesis we cannot be absolutely sure that the conductivity has improved, even though it looks like it. The effect of adding

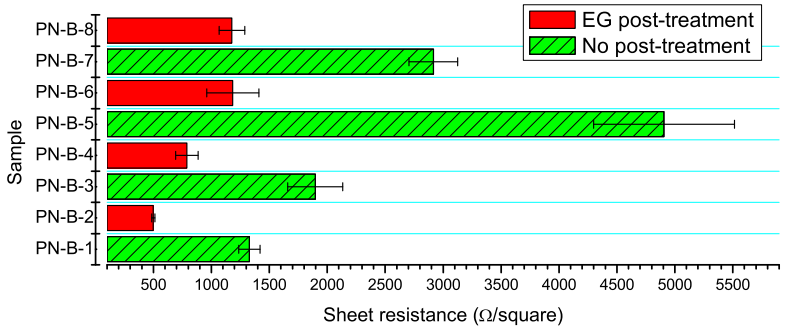

Figure 8.6. *Sheet resistance values of PEDOT:PSS/CNT samples applied with CX202 motorized bar coater. The error bars express the STDEV of sheet resistance values.*

CNTs into PEDOT:PSS has earlier been studied by Yun et al. [54]. They found the reduction in sheet resistance as well when CNTs were added.

The problems that were faced in flexographic printing of silver inks led to non-uniform films on any of used substrates. No sheet resistance values were received for any of the flexo printed silver samples (S-F-1, S-F-2 and S-F-3). Supposedly the conducting layer is not continuous. The only silver sample (S-B-1) on PVDF that was fabricated with CX202 had fairly low sheet resistance on both sides of the substrate ((0.146 ± 0.016) Ω/□ and (0.749 ± 0.164) Ω/□).

For the carbon ink sample on PVDF (C-F-1) sheet resistance was also measured. Even though the carbon ink should be resistive ink, R_S values of its electrodes were rather low ((6.474 ± 1.641) kΩ/□ and (34.148 ± 17.476) kΩ/□). One reason that may lead to this result is that C-F-1 was printed a few times. This increases the film thickness and most likely C-F-1 is thicker than flexo printed CNT or PEDOT:PSS samples. Increased thickness leads to this low sheet resistance, even though it is printed with a resistive ink.

8.2 Results of sensitivity measurements

Sensitivity measurements of all the piezoelectric PVDF samples were made by our collaborator Ville Rantanen [29]. Each sample was measured at nine spots on both sides. 5 cm × 3 cm strips of metallized PVDF film (Products of Measurement Specialties Inc.) and a PVDF film with in-house evaporated 3 cm × 3 cm sized, 50 nm thick copper electrodes were used as reference samples. In sensitivity measurements the value of piezoelectric constant d_{33} of the samples was measured. Promising results for the flexo printed samples were achieved. Complete results of sensitivity

measurements can be found in table D.1 in appendix D. Figure 8.7 is drawn based on those results.

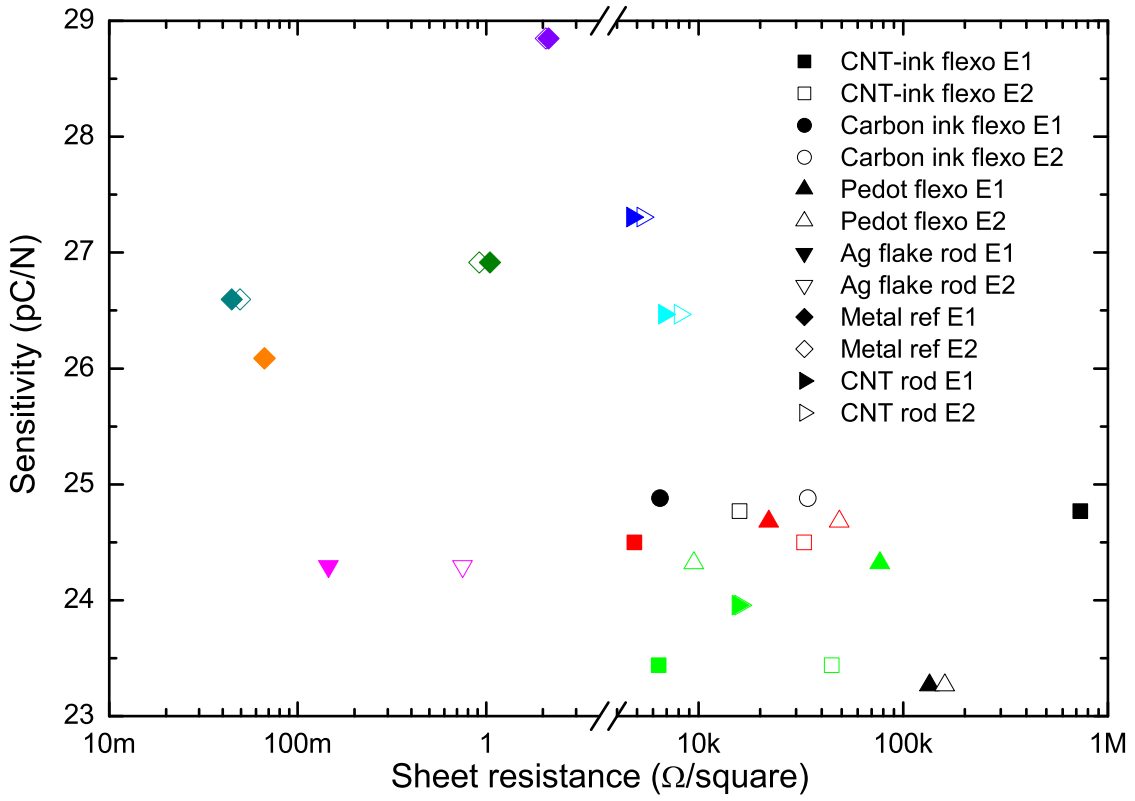

Figure 8.7. *Sheet resistance values of PEDOT:PSS/CNT samples applied with CX202 motorized bar coater. The error bars express the STDEV of sheet resistance values. Individual samples can be labelled by comparing their R_S and sensitivity values to those found in section 8.1 and appendix D.*

The dependence of samples' sensitivities on their sheet resistances is ambiguous. Clearly can be seen that when the sample has large R_S value its sensitivity value tends to be smaller. However, for samples having R_S less than 10 kΩ/□, the sensitivity can vary from 24 to 29 pC/N and the dependency of sensitivity on sheet resistance is far from being clear.

One thing that can be said about figure 8.7 is that even though the sheet resistance of a self-made sample is much larger than that of a reference sample, the sensitivity is only about 10 % smaller. Most likely this decrease in sensitivity does not prevent them from being used as sensitive pressure sensors.

8.3 Vibration resistance testing

Sensors may be exposed to vibrational stress during use and therefore their resistance to it may be worth testing. Samples were tested with an Espec corp. model EV-501 vibration shaker. Samples were put through a JESD-22-B103-3 service condition 1

test. It is a test with peak acceleration of 20 G and peak-to-peak displacement of 1.5 mm. Test starts from minimum frequency of 20 Hz and the frequency increases logarithmic to its maximum value of 2000 Hz and then returns logarithmic back to 20 Hz. One back and forth sweep takes four minutes and four of these sweeps are done for each sample. [57]

During the test, samples are fixed between two aluminum plates that are 120 mm in diameter and have a 30 mm hole in the middle for the sample to vibrate freely. The aluminum plates with the sample are then attached to the vibration shaker with six screws and the test is run.

Effect of the test on the sample is simply measured by comparing sheet resistances that are measured before and after the vibration exposure. If conducting film is removed from the sample during the test, it should increase the sheet resistance of the sample. Results of this test can be seen in figure 8.8. The sheet resistances values represented are lower ones of the two electrodes of the sample. The sheet resistances of the samples may differ from the ones that were measured and represented earlier in section 8.1. This is because sheet resistant measurements for vibration resistance testing were done much later. Aging is a problem at least for PEDOT:PSS samples. [48]

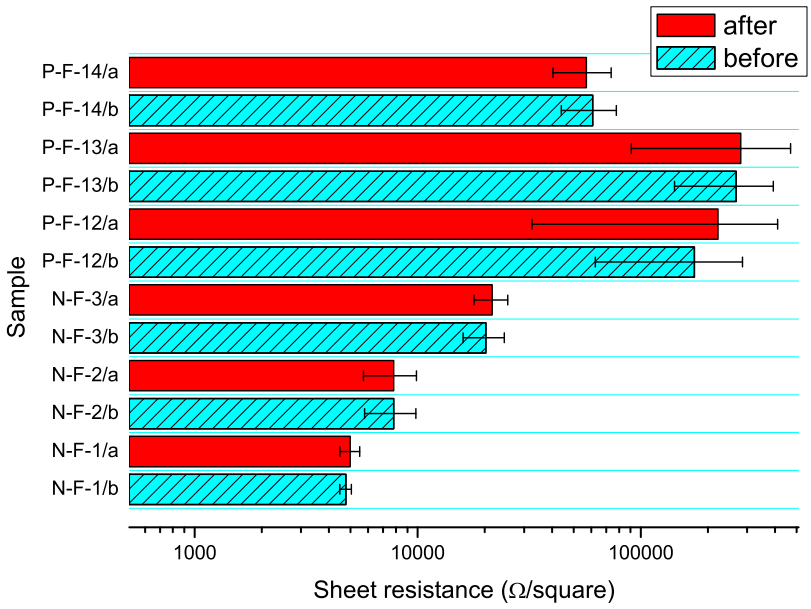

Figure 8.8. *Results of vibration test.*

One can clearly see that CNT and PEDOT:PSS samples resist vibration well. There are only small differences in sheet resistances. Small enough to fit within STDEV. This vibration test may not be the best way to test the samples, though.

Even though the maximum acceleration of 20 G is high, the forces that the conducting molecules experience are rather small due to their small mass. Too small to overcome the adhesive and cohesive forces that keep them in place.

8.4 Microscope and SEM pictures

As was mentioned earlier, thickness of the printed electrodes was really hard to measure. One way to do so is to take a cross-section picture of the sample. In order for the cross-section to be clean and clear the sample has to be mould into epoxy. Once the epoxy is dry the cross-section sample has to be ground and polished. However, this method appeared rather useless for most samples, because no clear film of ink could be distinguished in cross-sectional images except for silver ink. In figure 8.9 a) cross-section of N-F-1 sample is represented by optical microscope (OM) and scanning electron microscope (SEM). One cannot see any clear layer that would represent printed electrode between the PVDF (middle) and epoxy layers (sides).

In figure 8.9 b) cross-section of S-B-1 is represented by OM and SEM. In these images the silver layer is clearly visible and therefore some estimations of silver film thickness can be made. The film thickness of S-B-1 is around 10 µm. The silver layer is far from being uniform. Silver appears granular and the thickness of the film varies, depending on which spot and on which side the thickness of the film is evaluated.

One explanation for poor results in SEM imaging is poor contrast between substrate, epoxy and electrode material. The solid contents of the inks, except for silver ink, consist mainly of carbon and other light elements. When the ink dries on the substrate these solids remain, whereas solvents evaporate. Because also epoxy and PVDF consist of mainly light elements, the contrast between these three different substances is poor. Because silver is much heavier element it has bigger contrast between epoxy and PVDF and is therefore clearly visible in SEM images.

Other explanation could simply be the fact that the electrode is too thin to be clearly visible even in SEM image which should not be the case since the electrodes are expected to be at least a few hundreds of nm:s thick. Also the non-uniformity of the electrode may reduce its visibility in OM and SEM images.

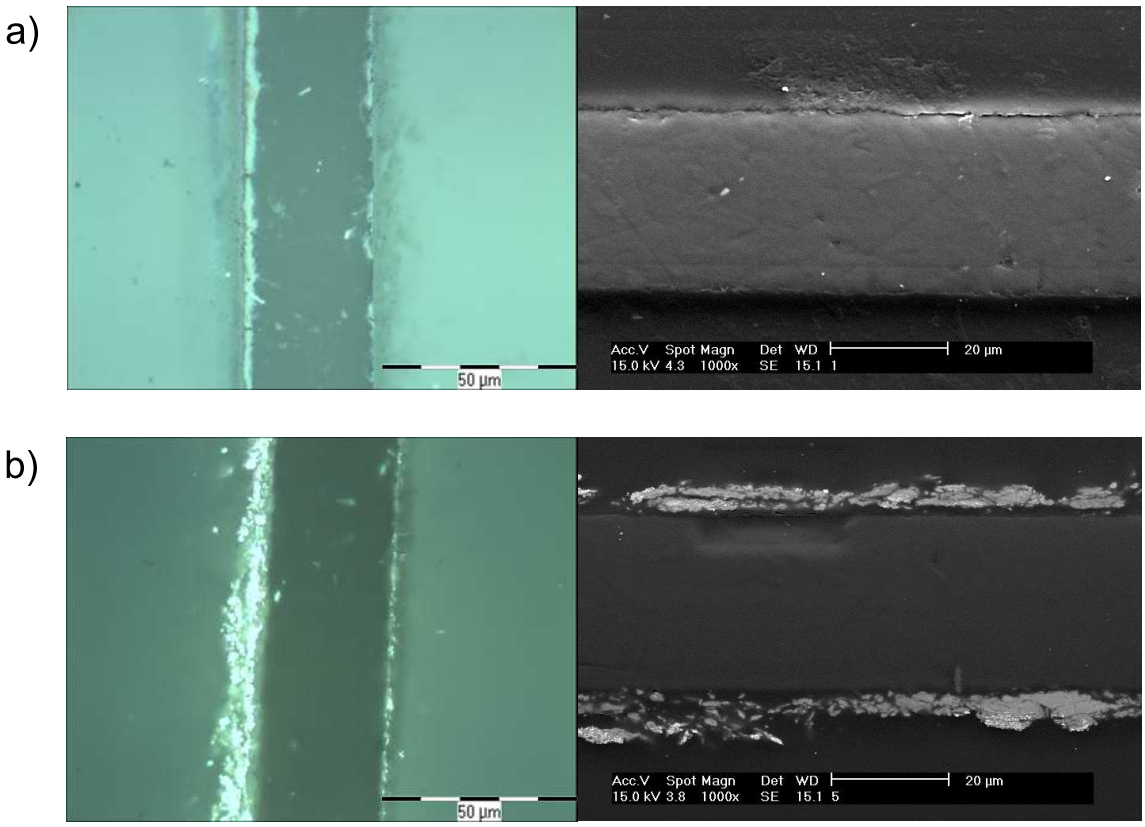

Figure 8.9. *Cross-sectional images of N-F-1 (a)) and S-B-1 (b)) samples taken with OM (left) and SEM (right).*

9. CONCLUSIONS

Results of the work done for this thesis are rather promising even though a lot of variance were observed in the results. Flexographic printing of uniform pressure sensors appeared difficult. However, in-house made sensors gave rather high response to applied normal force, despite of their non-uniform structure. Fairly good sensitivities were received for all electrode materials.

Poor printability of the electrodes with RK Flexiproof 100 was most likely caused by fast drying of the inks on anilox. Dried ink clogged the cells on anilox, reducing ink transfer to printing plate and further to the substrate. Reduced amount of ink equals thinner electrode and thus higher R_S value of the electrode. Difference in R_S values of two electrodes of same sample can be almost up to ten-fold. This problem caused by drying of ink can most likely be solved in full-scale press, in which the ink supply to the anilox is constant.

Other problem that was faced with flexographic printing was stripe formation. These stripes occurred in CNT and PEDOT:PSS samples and can be result of poor wetting. SDS was added to the inks to improve wetting. Also the fact that the "inks" used were really not inks, rather solutions, might result in poor printing quality. Real inks have plenty of additives that improve their printability. In this work only slight changes on solutions could be made.

CX202 motorized bar coater appeared to be a handy tool in studying different inks. Its speed and simplicity enabled much faster sample fabrication than RK Flexiproof 100. It also seemed to be able to produce thicker and more uniform films. One has to remember though, that CX202 is not a printer and therefore results achieved with it cannot be applied directly to flexographic mass production.

For CNT samples no clear dependency was found between ink formulation and R_S value. One interesting result that was achieved was the fact that when CNT samples were fabricated with CX202 the samples fabricated on PET had lower R_S values than the ones fabricated on PC. No reason for this phenomenon was found. Lowest achieved value of R_S with both fabrication methods was around 5 k$\Omega/\square$.

For PEDOT:PSS samples clear dependency was found between ink formulation and R_S value. Addition of SDS or high boiling solvents (EG or DMSO) decreased R_S values significantly. Addition of SDS into PEDOT:PSS ink reduced R_S value of fabricated film up to 68 times compared to film prepared with pure Baytron™ PH

500 PEDOT:PSS solution. By adding EG or DMSO or both the change was even more radical. The biggest reduction of R_S was 595 times compared to film prepared with pure Baytron™ PH 500.

Another way to reduce R_S values of PEDOT:PSS samples was to immerse fabricated samples into EG bath. Samples that were prepared with ink based on Clevios™ FE, EG post-treatment reduced R_S value up to 226 times when CX202 was used and up to 794 times when RK Flexiproof 100 was used. Lowest R_S value measured for flexo printed PEDOT:PSS sample was around 1.1 kΩ/□ and around 660 Ω/□ for samples fabricated with CX202.

Lowest R_S values all CNT and PEDOT:PSS samples were achieved with samples that were fabricated with PEDOT:PSS/CNT inks and EG post-treated afterwards. Lowest recorded R_S value was around 500 Ω/□. Unfortunately these results were not recorded on PVDF but on PET.

No clear dependency between R_S value and sensitivity was found, although it seems, in many cases, that the lower the R_S value the higher the sensitivity. Even though the R_S values of metallized reference samples were around two to three orders lower than those of our self-made CNT and PEDOT:PSS samples, difference in sensitivity was only around 10 %. These results are quite promising when these new materials are to be considered as new generation flexible electrode materials in piezoelectric pressure sensors. Because sensitivity measurements in this work were made with low frequency (2 Hz), further study has to be made before these sensors can be used in applications that require higher frequencies.

In conclusion, sensitivity results that were achieved are very promising. CNT and PEDOT:PSS inks are most likely suitable to be used as electrode materials on flexible PVDF piezoelectric pressure sensors. However printability of these materials has to be improved before they can be used in mass production by flexographic press.

REFERENCES

[1] M.A.M. Leenen, V. Arning, H. Thiem, J. Steiger, and R. Anselmann. Printable electronics: flexibility for the future. *Phys. Status Solidi A*, 206(4):588–597, 2009.

[2] S. Kärki, M. Kiiski, M. Mäntysalo, and J. Lekkala. A pvdf sensor with printed electrodes for normal and shear stress measurements on sole. *XIX IMEKO World Congress Fundamental and Applied Metrology September 6-9, 2009, Lisbon, Portugal*, pages 1765–1769, 2009.

[3] P. Viluksela, S. Ristimäki, and T. Spännäri. *Painoviestinnän tekniikka*. Opetushallitus, Keuruu, Finland, 2007.

[4] Flexography. http://www.wmich.edu/pci/flexo/. Online: Accessed 5-October-2011.

[5] P. Oittinen and H. Saarelma. *Papermaking Science and Technology: Printing*. Fapet Oy, Helsinki, Finland, 1998.

[6] Miraclon. http://www.rbcor.com/miraclon.htm. Online: Accessed 6-October-2011.

[7] Asahi. http://www.asahi-afp.com/En/web/catalog/about_afp_dsh_e.html. Online: Accessed 6-October-2011.

[8] Rk flexiproof 100. http://www.testingmachines.com/30-60-flexiproof-100.html. Online: Accessed 10-October-2011.

[9] Geoffrey Barnes and Ian Gentle. *Interfacial Science, An Introduction*. Oxford University Press Inc., New York, 2005.

[10] D. Gamota, P Brazis, K. Kalyanasundaram, and Zhang J. *Printed Organic and Molecular Electronics*. Kluwer Academic Publishers, Norwell, Massachusetts, 2004.

[11] Ken Gilleo. *Polymer Thick film*. Van Nostrand Reinhold, New York, 1996.

[12] Alain C. Diebold. *Handbook of Silicon Semiconductor Metrology*. Marcel Deccer, Inc., New York, 2001.

[13] Peter Van Zant. *Microchip Fabrication*. McGraw-Hill Companies, Inc., United States of America, 5th edition, 2004.

[14] Dieter K. Schroder. *Semiconductor Material and Device Characterization*. John Wiley & Sons, Inc., Hoboken, New Jersey, 3rd edition, 2006.

[15] Geometric factors in four point resistivity measurement. bulletin no. 472-13. http://www.fourpointprobes.com/haldor.html#hal. Online: Accessed 12-October-2011.

[16] Series 2400 sourcemeter line data sheet. http://www.keithley.com/products/dcac/currentvoltage/highcurrent/?path=2425/Documents#4. Online: Accessed 12-October-2011.

[17] Spring contact probes 2010 catalogue. http://www.feinmetall.de/fileadmin/user_upload/feinmetall/pdf/Downloads/en/Spring_Contact_Probes_2010.pdf. Online: Accessed 12-October-2011.

[18] Kenji Uchino and Jayne R. Giniewicz. *Micromechatronics*. Marcel Dekker Inc., New York, 2003.

[19] Ahmad Safari and E. Koray Akdogan. *Piezoelectric and Acoustic Materials for Transducer Applications*. Springer Science+Business Media, New York, 2008.

[20] S.O.R. Moheimani and A.J. Flemming. *Piezoelectric Transducers for Vibration Control and Damping*. Springer-Verlag, London, 2006.

[21] Marwin Webber. *Handbook of Optical Materials*. CRC Press 2003, Boca Raton, 2003.

[22] T. Furukawa. Piezoelectricity and pyroelectricity in polymers. *Electrical Insulation, IEEE Transactions on*, 24(3):375–394, 1989.

[23] Piezo Film Sensors Technical Manual, Measurement Specialties, Inc.

[24] M.A. Razian and M.G. Pepper. Design, development, and characteristics of an in-shoe triaxial pressure measurement transducer utilizing a single element of piezoelectric copolymer film. *Neural Systems and Rehabilitation Engineering, IEEE Transactions on*, 11(3):288–293, 2003.

[25] JS Harrison and Z. Ounaies. Piezoelectric polymers. *Encyclopedia Of Polymer Science and Technology*, 2002.

[26] A.J. Lovinger. Ferroelectric polymers. *Science*, 220(4602):1115, 1983.

[27] Manas Chanda and Salil K. Roy. *Plastics Technology Handbook*. CRC Press, Boca Raton, 4th edition, 2007.

[28] N.P. Rao, J. Dargahi, M. Kahrizi, and S. Prasad. Design and fabrication of a microtactile sensor. In *Electrical and Computer Engineering, 2003. IEEE CCECE 2003. Canadian Conference on*, volume 2, pages 1167–1170. IEEE, 2003.

[29] Department of Automation Science and Engineering, Tampere University of Technology (TUT), P.O. Box 692, FI-33101 Tampere, Finland.

[30] S. Iijima et al. Helical microtubules of graphitic carbon. *Nature*, 354(6348):56–58, 1991.

[31] Radushkevich L.V. and Lukyanovich V.M. *Zurn. Fisic. Chim.*, 111(24), 1952.

[32] Harold Hart, Leslie E. Craine, David J. Hart, and Christopher M. Hadad. *Organic Chemistry: A Short Course*. Houghton Mifflin Company, Boston, 12th edition, 2007.

[33] R. Saito, G. Dresselhaus, and M.S. Dresselhaus. *Physical Properties of Carbon Nanotubes*. Imperial College Press, London, 1998.

[34] J. Clayden, N. Greeves, S. Warren, and P. Wothers. *Organic Chemistry*. Oxford University Press, New York, 2001.

[35] M. Meyyappan. *Carbon Nanotubes Science and Applications*. CRC Press, Boca Raton, 2005.

[36] H. Nakahara. 3D Models of Carbon Nanotubes. http://www.surf.nuqe.nagoya-u.ac.jp. Online: Accessed 30-August-2011.

[37] Yury Gogotsi. *Carbon Nanomaterials*. CRC Press, Boca Raton, 2006.

[38] L. Jiang, L. Gao, and J. Sun. Production of aqueous colloidal dispersions of carbon nanotubes. *J. Colloid Interf. Sci.*, 260(1):89–94, 2003.

[39] W.H. Duan, Q. Wang, and F. Collins. Dispersion of carbon nanotubes with sds surfactants: a study from a binding energy perspective. *Chem. Sci.*, 2(7):1407–1413, 2011.

[40] P. Moilanen, M. Luukkainen, J. Jekkonen, and V. Kangas. Emi shielding effects of carbon nanotube cellulose nanocomposite. In *Electromagnetic Compatibility (EMC), 2010 IEEE International Symposium on*, pages 198–201. IEEE, 2010.

[41] D. Klemm, D. Schumann, F. Kramer, N. Heßler, D. Koth, and B. Sultanova. Nanocellulose materials–different cellulose, different functionality. In *Macromolecular Symposia*, volume 280, pages 60–71. Wiley Online Library, 2009.

[42] N. Minami, Y. Kim, K. Miyashita, S. Kazaoui, and B. Nalini. Cellulose derivatives as excellent dispersants for single-wall carbon nanotubes as demonstrated by absorption and photoluminescence spectroscopy. *Appl. Phys. Lett.*, 88:093123, 2006.

[43] What is nanocellulose? Presentation slides 14.2.2008. http://www.vtt.fi/kuvat/uutta/Nanocentre_LaineTKK.pdf. Online: Accessed 1-December-2011.

[44] W. M. Haynes. *CRC Handbook of Chemistry and Physics*. CRC Press/Taylor and Francis, Boca Raton, Florida, 92nd (internet version 2012) edition, 2011-2012.

[45] P. Chandrasekhar. *Conducting polymers, fundamentals and applications: a practical approach*. Springer Netherlands, 1999.

[46] A.J. Heeger. Nobel lecture: Semiconducting and metallic polymers: The fourth generation of polymeric materials. *Rev. Mod. Phys.*, 73(3):681–700, 2001.

[47] JY Kim, JH Jung, DE Lee, and J. Joo. Enhancement of electrical conductivity of poly (3, 4-ethylenedioxythiophene)/poly (4-styrenesulfonate) by a change of solvents. *Synthetic Met.*, 126(2-3):311–316, 2002.

[48] Y.H. Kim, C. Sachse, M.L. Machala, C. May, L. Müller-Meskamp, and K. Leo. Highly conductive pedot: Pss electrode with optimized solvent and thermal post-treatment for ito-free organic solar cells. *Adv. Funct. Mater.*

[49] B. Fan, X. Mei, and J. Ouyang. Significant conductivity enhancement of conductive poly (3, 4-ethylenedioxythiophene): Poly (styrenesulfonate) films by adding anionic surfactants into polymer solution. *Macromolecules*, 41(16):5971–5973, 2008.

[50] Nanoscience Center, University of Jyväskylä (JYU), P.O. Box 35, 40014 Jyväskylän yliopisto, Finland.

[51] Clevios™ FE data sheet. http://clevios.com/en/_technik/productdetail_1034001.aspx?psMarketId=1280&psApplicationId=. Online: Accessed 25-October-2011.

[52] Clevios™ PH 500 data sheet. http://clevios.com/en/_technik/productdetail_1034021.aspx?psMarketId=1280&psApplicationId=. Online: Accessed 25-October-2011.

[53] S. Tuukkanen, T. Julin, V. Rantanen, P. Moilanen, K.E. Lilja, and S. Rajala. Low-temperature processed printed electrodes for a piezoelectric thin film pressure sensor. *Submitted for publishing in February 2012*, 2012.

[54] D.J. Yun, K.P. Hong, S. Kim, W.M. Yun, J. Jang, W.S. Kwon, C.E. Park, and S.W. Rhee. Multiwall carbon nanotube and poly (3, 4-ethylenedioxythiophene): Polystyrene sulfonate (pedot: Pss) composite films for transistor and inverter devices. *ACS Applied Materials & Interfaces*, 2011.

[55] Solid surface energy data (SFE) for common polymers. http://www.surface-tension.de/solid-surface-energy.htm. Online: Accessed 25-October-2011.

[56] A. Elschner and W. Lövenich. Solution-deposited PEDOT for transparent conductive applications. *MRS Bull.*, 36, 2011.

[57] JEDEC STANDARD, Vibration, Variable Frequency, JESD22-B103B. http://www.jedec.org/sites/default/files/docs/22b103b.pdf. Online: Accessed 3-November-2011.

A. APPENDIX: INK FORMULATIONS

Table A.1. *CNT base solutions used in this thesis.*

Solution	Composition
Nano-1	CNT-nanocellulose nanocomposite, CNT:CMC 50:50, solids content 2 %, solvent: water
Nano-2	CNT-CMC composite, 60:40 CNT:CMC, solids content 0.8 %, solvent: H_2O:EtOH 1:1
Nano-3	CNT-CMC composite, 60:40 CNT:CMC, solids content 1.0 %, solvent: H_2O:EtOH 1:0.x
Nano-4	CNT-nanocellulose nanocomposite, CNT:CMC 50:50, solids content 4.14 %, solvent: water
Nano-5	CNT-nanocellulose nanocomposite, CNT:CMC 50:50, solids content 2.48 %, solvent: water
Nano-6	CNT-CMC composite, 60:40 CNT:CMC, solids content 1.7 %, solvent: H_2O:EtOH 1:1

Table A.2. *CNT ink formulations used in this thesis.*

Ink	CNT solution	Solution volume (ml)	2 % SDS (ml)	5 % SDS (ml)	IPA (ml)
CNT-1	Nano-4	5.00		0.20	
CNT-2	Nano-5	5.00		0.20	
CNT-3	Nano-2	5.00		0.10	
CNT-4	Nano-1	3.00		0.15	
CNT-5	Nano-3	3.00		0.15	
CNT-6	Nano-1	3.00			1.00

Table A.3. *Silver ink formulations used in this thesis.*

Ink	Electrodag PM-460A (g)	PGMEA (g)
Ag-1	11.926	6.5916
Ag-2	7.1260	7.3767
Ag-3	11.4948	8.0707

Table A.4. *PEDOT:PSS ink formulations based on Clevios™ FE.*

Ink	Clevios™ FE (g)	5 % SDS (g)	IPA (g)	P-1 (g)	EG (g)
PED-1	5.0010		3.7581	1.2787	
PED-2	5.0675		3.7880	1.2758	1.0260
PED-3	3.0000	0.88			
PED-4	3.0000	0.50			
PED-5	3.00	0.20		0.3142	
PED-6	2.4990		1.8805	0.6328	

Table A.5. *PEDOT:PSS ink formulations based on Baytron™ PH 500.*

Ink	Clevios™ PH 500 (ml)	10 % SDS (ml)	EG (ml)	DMSO (ml)
PED-7	2.85		0.15	
PED-8	2.85			0.15
PED-9	2.70		0.15	0.15
PED-10	3.00	0.20		
PED-11	2.28	0.20	0.12	
PED-12	2.28	0.20		0.12
PED-13	2.16	0.20	0.12	0.12

Table A.6. *PEDOT:PSS/CNT ink formulations.*

Ink	Nano-1 (ml)	Clevios™ FE (ml)	5 % SDS (ml)
PEDCNT-1	0.30	2.70	
PEDCNT-2	0.30	2.70	0.50
PEDCNT-3	0.60	2.40	
PEDCNT-4	0.60	2.40	0.50

B. APPENDIX: FLEXO PRINTED SAMPLES

Table B.1. *CNT samples fabricated with RK Flexiproof 100.*

Sample	Ink	Substr.	Plate	Anilox (cm^3/m^2)	Sample fabrication
N-F-1	CNT-1	PVDF	A	20.2	Washed with IPA, 5 min UV ozone both sides.
N-F-2	CNT-2	PVDF	A	20.2	Washed with IPA, 5 min UV ozone both sides.
N-F-3	CNT-3	PVDF	A	14.1	Washed with IPA, 5 min UV ozone both sides.

Table B.2. *PEDOT:PSS samples fabricated with RK Flexiproof 100.*

Sample	Ink	Substrate	Sample post-treatment
P-F-1	PED-4	PET	No post treatment
P-F-2	PED-4	PET	3 min glycol bath, 20 min in 120 °C oven.
P-F-3	PED-4	PET	3 min glycol bath, 75 min in 70 °C oven.
P-F-4	PED-4	PC	No post-treatment
P-F-5	PED-4	PC	3 min glycol bath, 20 min in 120 °C oven.
P-F-6	PED-4	PC	3 min glycol bath, 75 min in 70 °C oven.
P-F-7	PED-1	PC	3 min glycol bath, 75 min in 70 °C oven.
P-F-8	PED-5	PET	3 min glycol bath, 75 min in 70 °C oven.
P-F-9	PED-5	PC	3 min glycol bath, 75 min in 70 °C oven.
P-F-10	PED-5	PET	No post-treatment
P-F-11	PED-5	PC	No post-treatment
P-F-12	PED-6	PVDF	No post-treatment
P-F-13	PED-3	PVDF	No post-treatment
P-F-14	PED-5	PVDF	No post-treatment

Table B.3. *Carbon and silver ink samples fabricated with RK Flexiproof 100.*

Sample	Ink	Substr.	Plate	Anilox (cm^3/m^2)	Sample fabrication
C-F-1	C-ink	PVDF	M	20.2	Washed with IPA, 5 min UV ozone both sides.
S-F-1	Ag-1	PVDF	M	14.1	Washed with IPA, 5 min UV ozone both sides.
S-F-2	Ag-2	PVDF	M	20.2	Washed with IPA, 5 min UV ozone both sides.
S-F-3	Ag-3	PVDF	M	20.2	Washed with IPA, 5 min UV ozone both sides.

C. APPENDIX: SAMPLES PREPARED WITH BAR COATER

Table C.1. *CNT samples fabricated with CX202 motorized bar coater.*

Sample	Ink	Substrate	Rod (µm)	Sample fabrication
N-B-1	Nano-1	PET	6	Washed with IPA, 5 min UV ozone.
N-B-2	Nano-1	PC	6	Washed with IPA, 5 min UV ozone.
N-B-3	Nano-2	PET	6	Washed with IPA, 5 min UV ozone.
N-B-4	Nano-2	PC	6	Washed with IPA, 5 min UV ozone.
N-B-5	Nano-3	PET	6	Washed with IPA, 5 min UV ozone.
N-B-6	Nano-3	PC	6	Washed with IPA, 5 min UV ozone.
N-B-7	CNT-4	PET	6	Washed with IPA, 5 min UV ozone.
N-B-8	CNT-4	PC	6	Washed with IPA, 5 min UV ozone.
N-B-9	CNT-5	PET	6	Washed with IPA, 5 min UV ozone.
N-B-10	CNT-5	PC	6	Washed with IPA, 5 min UV ozone.
N-B-11	CNT-6	PVDF	6	Washed with IPA, 5 + 5 min UV ozone.
N-B-12	Nano-2	PVDF	6	Washed with IPA, 5 + 5 min UV ozone.
N-B-13	Nano-6	PVDF	6	Washed with IPA, 5 + 5 min UV ozone.

Table C.2. *PEDOT:PSS samples fabricated with CX 202 motorized bar coater.*

Sample	Ink	Substrate	Rod (µm)	Sample fabrication
P-B-1	PED-1	PET	12	Washed with IPA, 5 min UV ozone.
P-B-2	PED-1	PET	12	Washed with IPA.
P-B-3	PED-1	PET	6	Washed with IPA, 5 min UV ozone.
P-B-4	PED-1	PET	6	Washed with IPA.
P-B-5	PED-1	PET	4	Washed with IPA, 5 min UV ozone.
P-B-6	PED-1	PET	4	Washed with IPA.
P-B-7	PED-2	PET	12	Washed with IPA, 5 min UV ozone.
P-B-8	PED-2	PET	10	Washed with IPA, 5 min UV ozone.
P-B-9	PED-2	PET	6	Washed with IPA, 5 min UV ozone.
P-B-10	PED-2	PET	4	Washed with IPA, 5 min UV ozone.
P-B-11	PED-3	PET	12	Washed with IPA, 5 min UV ozone.
P-B-12	PED-3	PET	10	Washed with IPA, 5 min UV ozone.
P-B-13	PED-3	PET	6	Washed with IPA, 5 min UV ozone.
P-B-14	PED-3	PET	4	Washed with IPA, 5 min UV ozone.
P-B-15	PED-3	PET	6	Washed with IPA, 5 min UV ozone.
P-B-16	PED-3	PET	6	Washed with IPA, 5 min UV ozone, after printing 20 min in 120 °C oven.
P-B-17	PED-3	PET	6	Washed with IPA, 5 min UV ozone, after printing 3 min glycol bath, 20 min in 120 °C oven.
P-B-18	PED-3	PET	6	Washed with IPA, 5 min UV ozone, after printing 20 min in 120 °C oven, 3 min glycol bath 20 min in 120 °C oven.

Table C.3. *PEDOT:PSS samples fabricated with CX 202 motorized bar coater.*

Sample	Ink	Substrate	Rod (µm)	Sample pretreatment
P-B-19	PH500	PET	6	Washed with IPA, 5 min UV ozone.
P-B-20	PED-7	PET	6	Washed with IPA, 5 min UV ozone.
P-B-21	PED-8	PET	6	Washed with IPA, 5 min UV ozone.
P-B-22	PED-9	PET	6	Washed with IPA, 5 min UV ozone.
P-B-23	PED-10	PET	6	Washed with IPA, 5 min UV ozone.
P-B-24	PED-11	PET	6	Washed with IPA, 5 min UV ozone.
P-B-25	PED-12	PET	6	Washed with IPA, 5 min UV ozone.
P-B-26	PED-13	PET	6	Washed with IPA, 5 min UV ozone.
P-B-27	PED-10	PET	6	5 min UV ozone.
P-B-28	PED-11	PET	6	5 min UV ozone.
P-B-29	PED-12	PET	6	5 min UV ozone.
P-B-30	PED-13	PET	6	5 min UV ozone.

Table C.4. *PEDOT:PSS/CNT samples fabricated with CX 202 motorized bar coater.*

Sample	Ink	Substrate	Rod (µm)	Sample fabrication
PN-B-1	PEDCNT-1	PET	6	Washed with IPA, 5 min UV ozone.
PN-B-2	PEDCNT-1	PET	6	Washed with IPA, 5 min UV ozone, after printing 3 min glycol bath, 35 min in 120 °oven.
PN-B-3	PEDCNT-2	PET	6	Washed with IPA, 5 min UV ozone.
PN-B-4	PEDCNT-2	PET	6	Washed with IPA, 5 min UV ozone, after printing 3 min glycol bath, 35 min in 120 °oven.
PN-B-5	PEDCNT-3	PET	6	Washed with IPA, 5 min UV ozone.
PN-B-6	PEDCNT-3	PET	6	Washed with IPA, 5 min UV ozone, after printing 3 min glycol bath, 35 min in 120 °oven.
PN-B-7	PEDCNT-4	PET	6	Washed with IPA, 5 min UV ozone.
PN-B-8	PEDCNT-4	PET	6	Washed with IPA, 5 min UV ozone, after printing 3 min glycol bath, 35 min in 120 °oven.

D. APPENDIX: RESULTS OF SENSITIVITY MEASUREMENTS

Table D.1. *Sensitivity measurements.*

Sample	Static force (N)	Dynamic force (N)	Sensitivity (pC/N)
N-F-1	3.043 ± 0.045	1.306 ± 0.021	24.500 ± 0.788
N-F-2	3.017 ± 0.065	1.256 ± 0.026	23.440 ± 3.438
N-F-3	3.071 ± 0.040	1.287 ± 0.022	24.769 ± 1.237
N-B-13	2.983 ± 0.041	1.346 ± 0.016	23.955 ± 2.096
N-B-14	2.979 ± 0.037	1.222 ± 0.034	27.306 ± 2.494
N-B-15	2.979 ± 0.070	1.340 ± 0.028	26.467 ± 1.790
P-F-12	3.068 ± 0.042	1.296 ± 0.026	23.268 ± 1.642
P-F-13	3.043 ± 0.042	1.278 ± 0.009	24.680 ± 1.846
P-F-14	3.011 ± 0.054	1.262 ± 0.011	24.322 ± 2.616
C-F-1	2.979 ± 0.036	1.289 ± 0.018	24.882 ± 1.399
S-B-1	2.986 ± 0.040	1.314 ± 0.024	24.292 ± 2.823
Evap. Cu	2.993 ± 0.017	1.292 ± 0.029	26.916 ± 1.640
28 µm Ag	2.994 ± 0.031	1.319 ± 0.019	26.595 ± 0.851
110 µm Ag	3.011 ± 0.037	1.334 ± 0.016	26.089 ± 0.957
28 µm CuNi	3.003 ± 0.037	1.317 ± 0.023	16.591 ± 1.116
110 µm CuNi	3.005 ± 0.037	1.334 ± 0.028	28.847 ± 2.452